

H₈Si₈O₁₂: A Model for the Vibrational Structure of Zeolite A

Martin Bärtsch, Peter Bornhauser, Gion Calzaferri,* and Roman Imhof

Institute for Inorganic and Physical Chemistry, University of Berne, Freiestrasse 3, CH-3000 Bern 9, Switzerland

*Received: September 20, 1993**

The vibrational structure of the highly symmetrical octahydridosilasesquioxane has been investigated in detail, and a harmonic force field in terms of internal force constants has been determined, based on extensive IR and FT-Raman data and on a normal coordinate analysis of H₈Si₈O₁₂ and D₈Si₈O₁₂. Group frequencies have been assigned according to a potential energy analysis, and relations to group frequencies of comparable silicon compounds have been discussed. A step by step procedure starting from O_h-H₈Si₈O₁₂ to the frameworks O_h-(O)₈Si₈O₁₂, D_{4h}-(O)₈Si₈O₁₂, D_{4h}-(≡SiO)₈Si₈O₁₂, and finally to D_{2d}-(≡TO)₈T₈O₁₂, T = Si or Al and Si/Al = 1, has turned out to be an excellent, enlightening approach for qualitatively and quantitatively describing the vibrational structure of the zeolite A framework. NIR FT-Raman spectra of Na⁺-exchanged zeolite Y and of Na⁺- and Ag⁺-exchanged zeolite A have been measured and compared with each other. An improved force field is reported, and a correlation of the experimental and the calculated IR and Raman spectra of zeolite A has allowed one to assign group frequencies to all fundamental modes. All fundamentals between 1110 and 950 cm⁻¹ belong to antisymmetric T-O-T stretching vibrations while the symmetric T-O-T stretching modes are at 860-830 cm⁻¹, 740-680 cm⁻¹, and 610-570 cm⁻¹. The fundamentals between 490 and 100 cm⁻¹ can be described as O-T-O bending vibrations—with the exception of a double four ring and two sodalite cage breathing modes and the 8-ring pore opening—whereas the T-O-T bending vibrations and the torsional modes are below 100 cm⁻¹.

I. Introduction

The aluminosilicate framework of zeolite A is generated by placing cubic T₈O₁₂ double four rings (D4R) in the centers of the edges of a cube of edge 12.3 Å connected by oxygen bridges.¹ Half of the T atoms are Si and the other half are Al according to Löwenstein's rule. The center of the unit cell is a large cavity with a free diameter of about 11 Å; 8-membered rings with a free diameter of 4.1 Å give access to the large cavity. The relation between the D4R and the zeolite A structure is shown in the first step of Scheme 1. The bridging oxygen atoms are omitted, as usual in this kind of drawing.² They have been added in the next step of this scheme which leads to the H₈Si₈O₁₂ molecule. This molecule appears as an excellent model for studying properties of the D4R secondary building unit. Its structure was first determined by Larsson³ and has lately been reinvestigated with special emphasis on the flexibility of the Si-O-Si bridge.⁴ The electronic structure of H₈Si₈O₁₂ is known,⁵ and its vibrational properties have been investigated to some extent.⁶⁻⁸

Understanding the vibrational spectra, the dynamics, and the transport properties of a zeolite framework demands a correct description of the vibrational behavior of these extended porous systems. A number of theoretical studies have been reported.^{9,10} Flanigen and co-workers described the first reliable classification of the infrared active vibrations of zeolites,¹¹ and Angell has contributed Raman spectra of several types of zeolites,¹² while No and co-workers have modeled the normal modes and frequencies of zeolite A by applying the pseudolattice method to the D4R subunit.¹³ Our understanding of the vibrational structure of zeolites and our capability to describe their properties are far from satisfactory, despite this. The force constants and therefore the force fields used are often insufficient, mainly because of the lack of good experimental data. If a molecular modeling approach should become successful, however, a good force field is needed. We have taken a new approach by measuring and interpreting the IR and the FT-Raman spectra of H₈Si₈O₁₂ and of D₈Si₈O₁₂ in detail, and we have determined an accurate harmonic force

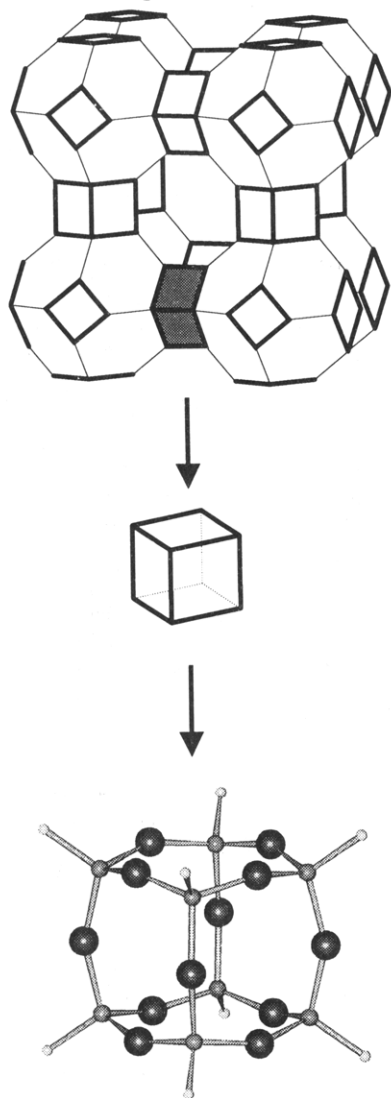
field of these molecules in terms of internal force constants. We have then applied these force constants for describing the vibrational structure of O_h-(O)₈Si₈O₁₂, D_{4h}-(O)₈Si₈O₁₂, D_{4h}-(≡SiO)₈Si₈O₁₂, and finally D_{2d}-(≡TO)₈T₈O₁₂, T = Si or Al and Si/Al = 1. This forms a basis to correlate the H₈Si₈O₁₂ molecule with the zeolite A, for which FT-Raman spectra are reported. Remarkable insight is gained by this approach, which not only simplifies the problem but also provides us with a much better justified force field.

II. Experimental Section

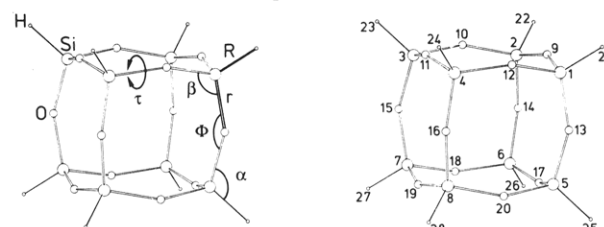
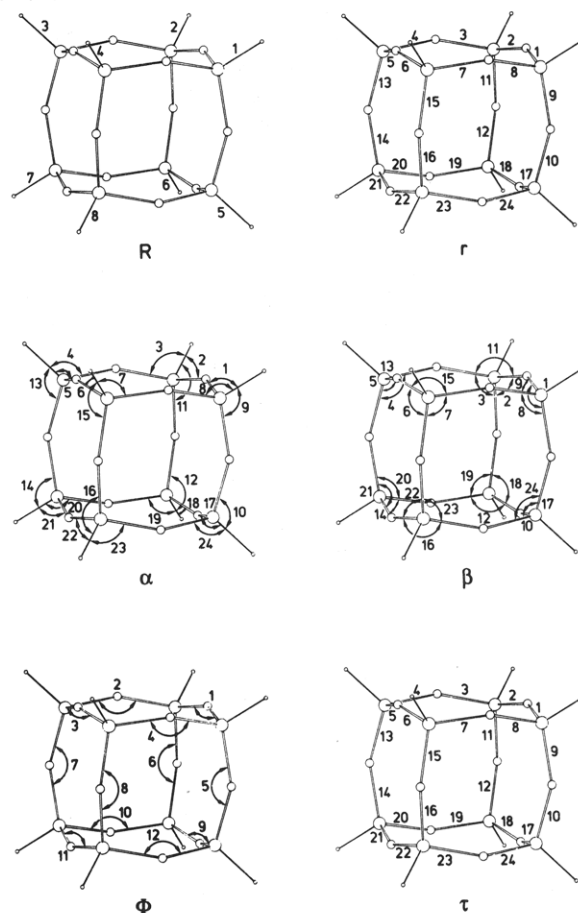
Sample Preparation. The octahydridosilasesquioxane H₈Si₈O₁₂ was synthesized and purified according to ref 14. Deuteration of this compound was done following the procedure of ref 15 with two minor changes: the Pd/C 10% catalyst was heated at 200 °C under vacuum (1 Pa) for 6 h and the reaction mixture was filtered using a milipore filter (type GV, 0.22 μm). Single crystals of H₈Si₈O₁₂ were prepared by very slow evaporation of a H₈-Si₈O₁₂/hexane solution. The zeolite Na-A (Linde 4A) was used as purchased from Bayer as Baylith T. Zeolite Na-Y was prepared according to the procedure described in ref 16 which leads to very pure Na-Y powder with a Si/Al ratio of 2.75. Ag-A was prepared by ion exchange 3 times with stoichiometric amounts of AgNO₃ (0.1 M) at pH 6 in the dark. Ag-A samples were always handled in the dark. Before and after ion exchange the zeolite was washed several times with bidistilled water.

Infrared and FT-Raman Spectra. The IR spectra were recorded on a Bomem DA3.01 FTIR spectrometer equipped with a liquid nitrogen cooled MCT detector (700-5000 cm⁻¹) and a liquid helium cooled CuGe detector (350-4000 cm⁻¹). A KBr beam splitter was applied for the measurements above 700 cm⁻¹, whereas in the range 350-700 cm⁻¹ a 3-μm Mylar beam splitter was used. The transmission IR spectra of H₈Si₈O₁₂ and of D₈Si₈O₁₂ shown in Figure 1 were measured in CCl₄ at room temperature with a resolution of 0.5 cm⁻¹. The spectrum of H₈Si₈O₁₂ was interpolated between 720 and 840 cm⁻¹, whereas D₈Si₈O₁₂ was measured in pentane in this region.

* Abstract published in *Advance ACS Abstracts*, February 1, 1994.

SCHEME 1: Relation between the Structure of Zeolite A, the D4R Double Four Ring, and the $H_8Si_8O_{12}$ Molecule

The FT-Raman spectra were recorded with the Bomem Raman accessory of the same FTIR spectrometer. The interferometer was equipped with a quartz beam splitter and a liquid nitrogen cooled InGaAs detector. The cw-Nd³⁺:YAG laser (Quantronix Model 114) was run in the TEM₀₀ mode at 9395 cm⁻¹. Rayleigh scattering was blocked either by different sets of Rayleigh line filters depending on the spectral range to be measured or by two holographic super notch filters (Kaiser Optical Systems) in 0° angle position. The Raman scatter was collected by an ellipsoidal mirror (*f*/1-optics) which forms a 180° backscattering geometry. As sample holder served a 2-mm-thick eloxadized aluminium plate with a 1- or 2-mm-diameter hole in which the probe was slightly pressed. The 2-mm hole was used for the $H_8Si_8O_{12}$ and for the zeolite probes, the 1-mm one for the $D_8Si_8O_{12}$. To determine the totally symmetric Raman lines a mixture of $H_8Si_8O_{12}$ powder and cyclohexane was sealed in a Duran glass capillary, which was heated to 150 °C in order to solve the powder. The polarized measurements were then performed with linearly polarizing Polaroid (type HR) filters. Linearly polarized measurements on arbitrarily oriented single crystals were done with the same polarizing filters. The spectra of $H_8Si_8O_{12}$ and $D_8Si_8O_{12}$ were not intensity corrected. The spectrum of the former one nevertheless shows approximately the correct relative intensities because of the inherent filter characteristics of the holographic super notch filter, which displays constant transmittance over the whole spectral range with the exception of the

SCHEME 2: Structure of $H_8Si_8O_{12}$ with Internal Coordinates and Numbering of the Atoms**SCHEME 3: Numbering of the Internal Coordinates of $H_8Si_8O_{12}$** 

cutoff region between about 9290 and 9570 cm⁻¹. The cutoff region may be shifted by slightly tuning the filters.^{17,18}

Calculations. The vibrational analysis of the investigated molecules was performed by the Wilson GF matrix method¹⁹ with the computer program package QCMP067.²⁰ Symmetry coordinates as reported in ref 6 have been applied. The correct elimination of the redundant internal symmetry coordinates was performed for each symmetry block separately.^{21,22}

III. Vibrations of $H_8Si_8O_{12}$ and $D_8Si_8O_{12}$

Structure and Internal Coordinates. The X-ray crystallographic analysis⁴ of $H_8Si_8O_{12}$ single crystals shows T_h symmetry for the Si_8O_{12} framework and S_6 symmetry for the eight H atoms. The deviation from O_h symmetry is small, the ¹H and ²⁹Si NMR spectra of $H_8Si_8O_{12}$ in solution consist each of a single line,²³ and the IR spectrum in solution is compatible with the O_h point group. We therefore start our analysis by assuming ideal octahedral symmetry of $H_8Si_8O_{12}$ and $D_8Si_8O_{12}$ with internal coordinates and numbering of the atoms as shown in Scheme 2. The numbering of the equivalent sets of internal coordinates is shown in Scheme 3.⁶ The 78 vibrational degrees of freedom of the

molecule are divided among the irreducible representations of the O_h point group according to:

$$\Gamma_{\text{vib}} = 3A_{1g} + A_{2g} + 4E_g + 3T_{1g} + 6T_{2g} + 3A_{2u} + 3E_u + 6T_{1u} + 4T_{2u} \quad (1)$$

From this follows that the molecule possesses 33 different fundamental modes, out of which 19 are triple degenerate, 7 double degenerate, and 7 nondegenerate. The selection rules tell us that the 6 $T_{1u} \leftarrow A_{1g}$ transitions are IR active; the 13 $A_{1g} \leftarrow A_{1g}$, $E_g \leftarrow A_{1g}$, and $T_{2g} \leftarrow A_{1g}$ transitions are Raman active; and the remaining 14 vibrations are inactive.

The Teller-Redlich product rule^{24,25} is a useful tool to prove an assignment of vibrations to a symmetry species. We will make use of this rule several times. It relates the vibrational frequencies ω_k and ω'_k of isotopic molecules and can be expressed for symmetry species γ with the dimension n in the following way:

$$\prod_{k=1}^n \frac{\omega'_k}{\omega_k} = \left[\prod_{i=1}^r \left(\frac{m_i}{m'_i} \right)^{n_i} \left(\frac{M'}{M} \right)^t \left(\frac{I'_x}{I_x} \right)^{d_x} \left(\frac{I'_y}{I_y} \right)^{d_y} \left(\frac{I'_z}{I_z} \right)^{d_z} \right]^{1/2} \quad (2)$$

In this expression m_i are the masses of the r equivalent sets s_i of atoms; M and M' are the masses of the isotopic molecules; and I_x , I_y , and I_z are the moments of inertia with respect to the appropriate principal axis. The symbols t , d_x , d_y , and d_z are the number of translations and rotations of the symmetry species γ , and n_i^γ is the number of irreducible representations γ which are generated by the equivalent set s_i of atoms. The dashed variable belong to the heavier isotopic molecule. This useful expression takes for the different symmetry types the following forms:

$$\begin{aligned} A_{1g}: \quad & \frac{\omega'_1 \omega'_2 \omega'_3}{\omega_1 \omega_2 \omega_3} = \left(\frac{m_H}{m_D} \right)^{1/2} \\ A_{2g}: \quad & \frac{\omega'_4}{\omega_4} = 1 \\ E_g: \quad & \frac{\omega'_5 \omega'_6 \omega'_7 \omega'_8}{\omega_5 \omega_6 \omega_7 \omega_8} = \left(\frac{m_H}{m_D} \right)^{1/2} \\ T_{1g}: \quad & \frac{\omega'_9 \omega'_{10} \omega'_{11}}{\omega_9 \omega_{10} \omega_{11}} = \left(\frac{m_H}{m_D} \right)^{1/2} \left(\frac{I_z^D}{I_z^H} \right)^{1/2} \\ T_{2g}: \quad & \frac{\omega'_{12} \omega'_{13} \omega'_{14} \omega'_{15} \omega'_{16} \omega'_{17}}{\omega_{12} \omega_{13} \omega_{14} \omega_{15} \omega_{16} \omega_{17}} = \left(\frac{m_H}{m_D} \right) \\ A_{2u}: \quad & \frac{\omega'_{18} \omega'_{19} \omega'_{20}}{\omega_{18} \omega_{19} \omega_{20}} = \left(\frac{m_H}{m_D} \right)^{1/2} \\ E_u: \quad & \frac{\omega'_{21} \omega'_{22} \omega'_{23}}{\omega_{21} \omega_{22} \omega_{23}} = \left(\frac{m_H}{m_D} \right)^{1/2} \\ T_{1u}: \quad & \frac{\omega'_{24} \omega'_{25} \omega'_{26} \omega'_{27} \omega'_{28} \omega'_{29}}{\omega_{24} \omega_{25} \omega_{26} \omega_{27} \omega_{28} \omega_{29}} = \left(\frac{m_H}{m_D} \right) \left(\frac{M^D}{M^H} \right)^{1/2} \\ T_{2u}: \quad & \frac{\omega'_{30} \omega'_{31} \omega'_{32} \omega'_{33}}{\omega_{30} \omega_{31} \omega_{32} \omega_{33}} = \left(\frac{m_H}{m_D} \right)^{1/2} \end{aligned} \quad (3)$$

Harmonic Force Field. The best description of the vibrational structure of a molecule from a chemical point of view is performed by a general valence force field in terms of internal coordinates

TABLE 1: Definition of the Simplified GVFF for H₈Si₈O₁₂^a

internal coordinate	R_1	r_1	r_2	r_8	α_1	α_8	β_1	β_8	Φ_1
R_1	f_R								
r_1	f_{Rr}	f_r							
r_2	0	f_{rr}	f_r						
r_8	f_{Rr}	f'_{rr}	0	f_r					
α_1	$f_{R\alpha}$	$f'_{r\alpha}$	0	$f'_{r\alpha}$	f_α				
α_8	$f_{R\alpha}$	$f'_{r\alpha}$	0	$f_{r\alpha}$	$f_{\alpha\alpha}$	f_α			
β_1	$f_{R\beta}$	$f'_{r\beta}$	0	$f'_{r\beta}$	$f_{\alpha\beta}$	$f'_{\alpha\beta}$	f_β		
β_8	$f_{R\beta}$	$f'_{r\beta}$	0	$f_{r\beta}$	$f'_{\alpha\beta}$	$f_{\alpha\beta}$	$f_{\beta\beta}$	f_β	
Φ_1	0	$f_{r\Phi}$	$f_{r\Phi}$	0	$f_{\alpha\Phi}$	0	$f_{\beta\Phi}$	0	f_Φ

^a $f'_{r\alpha}$, $f'_{r\beta}$, and $f'_{\alpha\beta}$ are interaction force constants belonging to internal coordinates which have no common bond, and f'_{rr} describes the interaction between two Si-O bond stretching coordinates with no common oxygen atom. τ and as a consequence f_τ are not included in this table; see text.

I_i and internal force constants f_{ij} . The potential energy function V in the harmonic approximation can then be expressed as

$$2V = \sum_i \sum_j f_{ij} I_i I_j \quad (4)$$

This force field is in general indeterminable, because the number of force constants exceeds the available experimental data. It is therefore necessary to introduce some simplifications. Three major simplifications can easily be accepted: interactions between bond stretching coordinates with no common atom can be neglected, interactions between angle bending coordinates α and/or β belonging to different silicon atoms are negligible, and interactions between a bond stretching coordinate and an angle bending coordinate α or β sharing no common silicon atom can be set equal to zero. In addition, interaction terms $f_{i\Phi}$ ($i = R, r, \alpha, \beta, \Phi$) with no common bond can be neglected. The torsional force constant f_τ is very small and is connected with the inactive A_{2g} mode only (see Table 5); therefore, it does not appear in our equations with the exception of the Appendix. Under these conditions the number of parameters is considerably reduced. Table 1 represents the resulting simplified general valence force field (GVFF) which consists of 21 different internal force constants.

Factorization of the secular equation is helpful to simplify the vibrational problem. The internal symmetry coordinates S_i , which factorize the secular equation to the maximum extent, are related to the internal coordinates I_i by the following unitary transformation:

$$S = UI \quad (5)$$

It has been shown that eq 5 results in 116 symmetry coordinates which have been tabulated in ref 6. The potential energy function in terms of these coordinates and the symmetry force constants F_{ij} is

$$2V = \sum_{i=1}^{116} \sum_{j=1}^{116} F_{ij} S_i S_j \quad (6)$$

It is necessary to divide the total of 116 symmetry coordinates into two groups, the nonredundant and the redundant ones. Although there is in general no unique choice of the nonredundant coordinates, the first restriction is given by the redundancy conditions among the coordinates in each symmetry block. These relations can be obtained by diagonalization of the G matrix according to²⁶

$$GD = D\Gamma \quad (7)$$

D represents a unitary matrix with the eigenvectors in their rows, and Γ is a diagonal matrix containing the eigenvalues. The redundancy conditions are then given by:

$$\mathbf{D}^T \mathbf{S} = \mathbf{0} \quad (8)$$

where \mathbf{D}^T is the transposed of \mathbf{D} . Applying this procedure, one can obtain the following relations:

A_{1g} :

$$S_3 + S_{R1} = 0$$

$$\sqrt{2}S_3 + S_{R2} = 0$$

T_{2g} :

$$\frac{1}{\sqrt{2}}S_{15} + \frac{1}{\sqrt{2}}S_{16} + S_{17} + S_{R6} = 0$$

$$kS_{13} + \frac{k\sqrt{2}}{10}S_{14} + \frac{\sqrt{2}}{6}S_{16} + \frac{4}{3}S_{17} + S_{R7} = 0 \quad (9)$$

A_{2u} :

$$S_{20} + S_{R10} = 0$$

T_{1u} :

$$\frac{1}{\sqrt{2}}S_{27} + S_{28} + \frac{1}{\sqrt{2}}S_{29} + S_{R12} = 0$$

$$\frac{k}{2}S_{25} + \frac{k\sqrt{2}}{10}S_{26} + \frac{5\sqrt{2}}{6}S_{28} + \frac{5}{6}S_{29} + S_{R13} = 0$$

The redundancy parameter k in these equations is equal to $1.028\ 807\ \text{\AA}^{-1}\ \text{rad}$. The choice of the nonredundant coordinates among the linearly dependent symmetry coordinates is to some extent arbitrary. We want to keep those coordinates which are easiest to visualize and which lead to the simplest expression for the potential energy function. This leads to the set of independent and normalized symmetry coordinates in Table 3 of ref 6 being used in the present study with the exception of S_3 and S_{20} , which have been replaced by S_{R1} and S_{R10} , respectively. The reason for this will be explained in the discussion.

The use of the nonredundant symmetry coordinates as described above requires proper transformation of the \mathbf{F} matrix, which means that the redundant coordinates in eq 6 must be substituted by a linear combination of the nonredundant ones according to the redundancy conditions (9).^{21,27} This leads to a new interpretation of the symmetry force constants F_{ij} . The new constants are named \mathcal{F}_{ij} and tabulated in the Appendix. The potential energy function in terms of the nonredundant symmetry coordinates and the corresponding force constants is:

$$2V = \sum_{i=1}^{78} \sum_{j=1}^{78} \mathcal{F}_{ij} S_i S_j \quad (10)$$

We now come back to Table 1 containing 21 different internal force constants. Analysis of the \mathcal{F}_{ij} leads to the result that some of the f_{ij} in Table 1 show linear dependencies. The coefficient matrix $\alpha\beta$ of the $f_{\alpha j}, f_{\beta j}$ ($j = \alpha, \beta$), and $f'_{\alpha\beta}$ as well as the coefficient matrix $r\alpha\beta$ of the f_{rj} and f'_{rj} ($j = \alpha, \beta$) are given in eq 11.

$$\alpha\beta = \begin{bmatrix} 1 & 2 & 1 & 2 & -4 & -2 \\ 1 & -1 & 0 & 0 & 0 & 0 \\ 0 & 0 & 1 & -1 & 0 & 0 \\ 0 & 0 & 0 & 0 & -1 & 1 \\ 1/2 & 1/2 & 1 & 0 & -2 & 0 \\ 1 & 1 & 1 & 1 & -2 & -2 \\ 1/2 & 1/2 & 0 & 1 & -3/2 & -1/2 \end{bmatrix}$$

$$r\alpha\beta = \begin{bmatrix} -1 & -2 & 2 & 1 \\ 1 & -1 & 0 & 0 \\ 0 & 0 & -1 & 1 \\ 0 & -1 & 0 & 1 \\ 0 & 1 & -1 & 0 \\ 1/2 & 1/2 & -1 & 0 \\ -1 & -1 & 1 & 1 \end{bmatrix} \quad (11)$$

The rank of $\alpha\beta$ is equal to four and that of $r\alpha\beta$ is equal to three. This means that out of the 10 f_{ij} only seven linear combinations are independent. Similar considerations reduce the number of independent f_{rj} ($j = \alpha, \beta$) by one. This reduces the number of different parameters to 17. The physically most reasonable set of such combinations is given in Table 5.

Infrared Spectra. We have already stated that for O_h - H_8 - Si_8O_{12} and also for O_h - D_8 - Si_8O_{12} six fundamental IR absorptions of T_{1u} symmetry should be observed. The spectra in Figure 1, however, show 10 easily identifiable bands for $H_8Si_8O_{12}$ and 14 in the case of $D_8Si_8O_{12}$, all reported in Table 2. Which of these bands are fundamentals and where do the extra bands come from? A glance at the T_{1u} symmetry coordinates reported in Table 3 of ref 6 tells us that one of the IR fundamentals is a Si-H stretching vibration, two are Si-O stretching modes, one is an O-Si-H bending, and two correspond to O-Si-O bending modes. The motions in which the H atoms are involved shift to lower energies when the H are replaced by D. All other modes of $H_8Si_8O_{12}$ and $D_8Si_8O_{12}$ should appear at about the same energies for the two molecules. From this we easily identify the bands at 2277 and 1659 cm^{-1} as Si-H and Si-D stretching, respectively, and those at 881 and 687 cm^{-1} as O-Si-H and O-Si-D bending, respectively. Siloxanes are known to show a characteristic strong absorption in the region of 1130–1000 cm^{-1} , assigned as antisymmetric Si-O-Si stretching frequency.^{28,29} It is therefore obvious that the absorptions at 1141 and 1140 cm^{-1} must be assigned to an antisymmetric Si-O-Si stretching mode. Symmetric Si-O-Si stretching frequencies have been reported between 625 and 480 cm^{-1} .^{30,36}

The assignment of the other fundamentals is less obvious and can only be made in a definite way by applying detailed normal coordinate analysis including all data available from the IR and Raman spectra as discussed below. We already know, however, that no splitting caused by symmetry lowering has been observed in the IR spectra of $H_8Si_8O_{12}$ and $D_8Si_8O_{12}$ measured in solution. This means that these spectra are consistent with O_h symmetry. The interpretation of all bands not arising from fundamentals are discussed later.

FT-Raman Spectra. Figure 2 shows the FT-Raman powder spectra of the octahydridosilasesquioxane $H_8Si_8O_{12}$ and its deuterated counterpart. The Raman lines of the two substances are collected in Table 3. Again more bands are observed than expected from the selection rules: 20 and 26 in the case of $H_8Si_8O_{12}$ and $D_8Si_8O_{12}$, respectively, instead of 13 in both cases.

In addition, two beautiful anti-Stokes lines (negative Raman shifts) are observed in the spectrum of $H_8Si_8O_{12}$. Observation of these lines was possible by applying holographic super notch filters whereas in the case of $D_8Si_8O_{12}$ dielectric filters were used. To eliminate the disturbing laser frequencies at 85 and 120 cm^{-1} which appear in the spectrum of $H_8Si_8O_{12}$, a special plasma line filter was used in the case of $D_8Si_8O_{12}$ which allows measurements down to 45 cm^{-1} . This enables one to prove that the 84- cm^{-1} line reported in ref 7 really belongs to a $H_8Si_8O_{12}$ vibration. In the spectrum of $H_8Si_8O_{12}$ the relatively weak 84- cm^{-1} line is superimposed by the 85- cm^{-1} laser line.

Out of the three $A_{1g} \leftarrow A_{1g}$, the four $E_g \leftarrow A_{1g}$, and the six $T_{2g} \leftarrow A_{1g}$ Raman lines, the totally symmetric A_{1g} vibrations of $H_8Si_8O_{12}$, for which depolarization measurements have been carried out, are readily identified at 2302, 580, and 456 cm^{-1} . The A_{1g} symmetry coordinates reported in Table 3 of ref 6 tell us that one of these fundamentals is a Si-H stretching vibration,

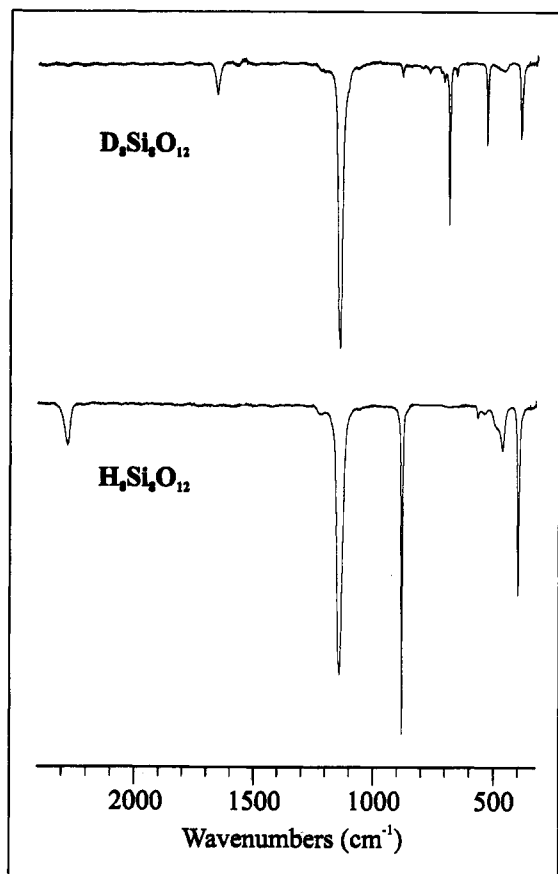


Figure 1. Transmission IR spectra of $\text{H}_8\text{Si}_8\text{O}_{12}$ and $\text{D}_8\text{Si}_8\text{O}_{12}$ measured in CCl_4 with a resolution of 0.5 cm^{-1} .

TABLE 2: Experimental IR Frequencies (cm^{-1}) of $\text{H}_8\text{Si}_8\text{O}_{12}$ and $\text{D}_8\text{Si}_8\text{O}_{12}$ with Their Assignments and Symmetries

$\text{H}_8\text{Si}_8\text{O}_{12}$	$\text{D}_8\text{Si}_8\text{O}_{12}$	assignment	symmetry
2277	1659	ν_{24}	T_{1u}
~ 1215	~ 1215	$\nu_{25} + \nu_8$	$T_{1u} + T_{2u}$
1141	1140	ν_{25}	T_{1u}
~ 1065	~ 1071	$\nu_{25} - \nu_8$	$T_{1u} + T_{2u}$
	881	$\text{HD}_7\text{Si}_8\text{O}_{12}$	E^a
	839	$\text{HD}_7\text{Si}_8\text{O}_{12}$	E^a
	770	$\text{HD}_7\text{Si}_8\text{O}_{12}$	E^a
	720	$\text{HD}_7\text{Si}_8\text{O}_{12}$	A_1^a
	710	$\text{HD}_7\text{Si}_8\text{O}_{12}$	E^a
881	687	ν_{26}	T_{1u}
	658	$\text{HD}_7\text{Si}_8\text{O}_{12}$	E^a
566	531	ν_{27}	T_{1u}
~ 537		$\nu_{28} + \nu_8$	$T_{1u} + T_{2u}$
~ 490		$\nu_{27} - \nu_8$	$T_{1u} + T_{2u}$
465	457	ν_{28}	T_{1u}
399	392	ν_{29}	T_{1u}

^a The symmetry labels are in accordance with the C_{3v} symmetry of $\text{HD}_7\text{Si}_8\text{O}_{12}$.

another one must correspond to a Si–O–Si stretching mode, and the third one to an O–Si–O bending. The first of them is expected to show a shift of approximately $2^{-1/2}$ in the case of $\text{D}_8\text{Si}_8\text{O}_{12}$, whose corresponding line has been observed at 1676 cm^{-1} .

Some of the six $T_{2g} \leftarrow A_{1g}$ Raman lines can be identified by considering the crystal symmetry, which is T_h for the Si_8O_{12} body and S_6 only for the whole molecule.⁴ This means that all those T_{2g} bands in which H atoms are involved are expected to split into A_g plus E_g while the others are not affected by the symmetry lowering. From this follows that the two lines at 2286 and 2296 cm^{-1} have to be identified as split Si–H stretching vibrations belonging to T_{2g} in $O_h\text{-H}_8\text{Si}_8\text{O}_{12}$, and it is easy to identify the corresponding lines at 1668 and 1660 cm^{-1} in the deuterated molecule. The other doublet at 883 and 897 cm^{-1} originates from the splitting of the T_{2g} band at 891 cm^{-1} measured in solution.

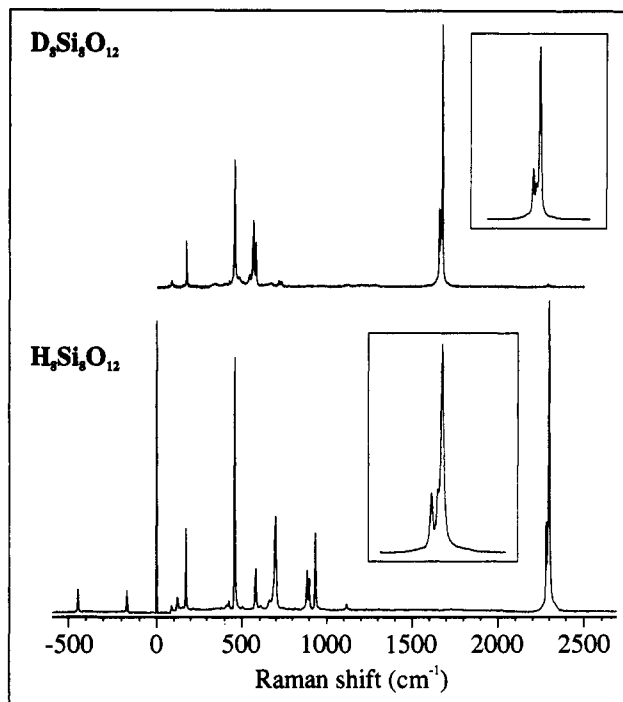


Figure 2. FT-Raman spectra of crystalline powder of $\text{H}_8\text{Si}_8\text{O}_{12}$ and $\text{D}_8\text{Si}_8\text{O}_{12}$. The intense signal at 0 cm^{-1} (9395 cm^{-1} on the absolute wavenumber scale) is the Nd:YAG laser excitation line. $\text{H}_8\text{Si}_8\text{O}_{12}$: 500-mW laser power, 100 scans, 4 cm^{-1} resolution. $\text{D}_8\text{Si}_8\text{O}_{12}$: 800-mW laser power, 500 scans, 1 cm^{-1} resolution. The two insets in each of the spectra show the enlarged regions of the $\nu(\text{Si-H})$ and $\nu(\text{Si-D})$ vibrations, respectively. The inset of the $\text{H}_8\text{Si}_8\text{O}_{12}$ spectrum originates from a measurement with a resolution of 1 cm^{-1} .

Its counterpart in the deuterated molecule appears at 729 and 713 cm^{-1} , respectively. This is supported by the product rule and an approximate calculation of the frequencies of these modes based on data of the symmetry blocks A_{1g} and T_{1u} . The other T_{2g} vibrations are not affected by the symmetry lowering in the crystal. Out of them the Si–O stretching at 1117 cm^{-1} (1115 cm^{-1} in $\text{D}_8\text{Si}_8\text{O}_{12}$) is readily recognized by applying the same arguments as for the IR active mode at 1141 cm^{-1} . An analysis with the product rule for all possible combinations of T_{2g} frequencies shows that the lines at 610 and 414 cm^{-1} of $\text{H}_8\text{Si}_8\text{O}_{12}$ and the corresponding frequencies at 541 and 405 cm^{-1} of $\text{D}_8\text{Si}_8\text{O}_{12}$ belong to T_{2g} . One vibration has still not been explained. We will show later that it appears at 171 cm^{-1} and corresponds to an O–Si–O bending mode.

We now focus on the four $E_g \leftarrow A_{1g}$ transitions. Again the E_g symmetry coordinates reported in Table 3 of ref 6 tell us that two of these fundamentals could be admixtures of O–Si–H bending and Si–O–Si stretching modes, another one an O–Si–O bending, and the fourth one a Si–O–Si bending. The first two of them are expected to show an isotope shift. Application of the product rule and an approximate calculation of the frequencies based on the data obtained in the symmetry blocks A_{1g} and T_{1u} allow the following tentative assignment. The strong lines at 697 cm^{-1} ($\text{H}_8\text{Si}_8\text{O}_{12}$) and 562 cm^{-1} ($\text{D}_8\text{Si}_8\text{O}_{12}$) belong to one of the E_g vibrations in which the H atoms are involved. It makes sense also to assume that the other E_g vibration in which the H atoms are involved appears at 932 cm^{-1} in the case of $\text{H}_8\text{Si}_8\text{O}_{12}$. The problem with this assignment is that no E_g counterpart in the $\text{D}_8\text{Si}_8\text{O}_{12}$ can be found. According to the product rule this line is expected to be above 820 cm^{-1} . Experimental observations give no indication for a Raman line in this region, however. It is indeed expected to be very weak, as will be discussed later. Normal coordinate analysis is needed to find out that the other E_g vibrations are at 423 and 84 cm^{-1} for $\text{H}_8\text{Si}_8\text{O}_{12}$ and at 422 and 84 cm^{-1} for $\text{D}_8\text{Si}_8\text{O}_{12}$.

TABLE 3: Experimental FT-Raman Frequencies (cm⁻¹) of H₈Si₈O₁₂ and D₈Si₈O₁₂ with Their Assignments and Symmetries

H ₈ Si ₈ O ₁₂	D ₈ Si ₈ O ₁₂	assignment	symmetry
2302		ν_1	A _{1g}
	2301	HD ₇ Si ₈ O ₁₂	A ^a
	2292	HD ₇ Si ₈ O ₁₂	A ^a
	1676	ν_1	A _{1g}
2296 } 2286 }	1668 } 1660 }	doublet ν_{12}	T _{2g}
	1283	$\nu_{13} + 2\nu_8$	T _{1g} + 2T _{2g}
	1203	$\nu_{13} + \nu_8$	T _{1g} + T _{2g}
1117	1115	ν_{13}	T _{2g}
	885	HD ₇ Si ₈ O ₁₂	A and E ^a
	877	HD ₇ Si ₈ O ₁₂	A ^a
	764	HD ₇ Si ₈ O ₁₂	A and E ^a
932		ν_5	E _g
897 } 883 }	729 } 713 }	doublet ν_{14}	T _{2g}
811		$\nu_{26} - \nu_{33}$	A _{2g} + E _g + T _{1g} + T _{2g}
697		ν_6	E _g
662	666	$\nu_2 + \nu_8$	E _g
610		ν_{15}	T _{2g}
	610	$\nu_{26} - \nu_{33}$	A _{2g} + E _g + T _{1g} + T _{2g}
580	579	ν_2	A _{1g}
	562	ν_6	E _g
	541	ν_{15}	T _{2g}
505	502	$\nu_7 + \nu_8$	A _{1g} + A _{2g} + E _g
	478	$\nu_6 - \nu_8$	A _{1g} + A _{2g} + E _g
456	452	ν_3	A _{1g}
423	422	ν_7	E _g
414	405	ν_{16}	T _{2g}
352	351	ν_{11}	T _{1g} ^b
171	170	ν_{17}	T _{2g}
84	84	ν_8	E _g
61		ν_4	A _{2g} ^b

^a The symmetry labels are in accordance with the C₃ or C₁ symmetry of HD₇Si₈O₁₂. ^b Inactive fundamentals which become Raman active due to symmetry lowering from O_h to T_h in the crystal.

TABLE 4: Intensity Ratios of Some Raman Lines of an Arbitrarily Oriented H₈Si₈O₁₂ Single Crystal

frequency (cm ⁻¹)	ratio (I _⊥ /I)	assignment
2302	0.17	A _{1g}
2286	0.22	split T _{2g} ^a
932	0.45	E _g
897 } 883 }	0.22 } 0.23 }	split T _{2g}
697	0.45	E _g
662	0.49	combination band (E _g)
579	0.17	A _{1g}
456	0.17	A _{1g}
423	0.50	E _g

^a Because of the 4-cm⁻¹ resolution, the second line is not resolved.

A further aid comes from polarized measurements of a H₈Si₈O₁₂ single crystal. Linearly polarized light is Raman scattered at different angles depending on the symmetry species of the vibrations. The ratio of the line intensities of polarized and unpolarized signals must be the same for vibrations belonging to the same irreducible representations within a point group and should differ for different symmetry species. Values observed by us of an arbitrarily oriented single crystal are reported in Table 4 and contain only values for which the error of the ratio is less than ±5%. The difference in the ratios observed for A_{1g}, E_g, and T_{2g} is so large that it can be taken as a strong indication for correct assignment.

Normal Coordinate Analysis. We start the quantitative analysis in terms of normal modes with the nonredundant internal symmetry coordinates and the corresponding force constants. This procedure helps one obtain the right assignment of the IR and Raman active fundamental modes of H₈Si₈O₁₂ and D₈Si₈O₁₂ because each symmetry block can be analyzed separately. Let us first try to describe the fundamentals by means of a diagonal

TABLE 5: Best Set of Internal Force Constants for H₈Si₈O₁₂ and D₈Si₈O₁₂

force constant	mdyn Å ⁻¹	mdyn Å rad ⁻²	mdyn rad ⁻¹
f_R	3.24		
f_r	5.10		
f_{rr}	0.275		
f'_{rr}	0.153		
$f_\alpha - f_{\alpha\alpha}$		0.601	
$f_\beta - f_{\beta\beta}$		0.895	
$f_{\alpha\beta} - f'_{\alpha\beta}$		0.079	
$f_{\alpha\alpha} + f_{\beta\beta} - 2f_{\alpha\beta}$		0.191	
$f_{r\alpha} - f'_{r\alpha}$			0.188
$f_{r\beta} - f'_{r\beta}$			-0.160
$f_{r\alpha} - f_{r\beta}$			0.204
f_ϕ		0.091	
$f_{r\phi}$			0.036
$f_{\alpha\phi}$		0.019	
$f_{\beta\phi}$		0.0026	
f_τ		0.0040 ^a	

^a See Table 11.

potential energy function:

$$2V = \sum_{\gamma} \sum_{n(\gamma)} \mathcal{F}_{nn} S_{nn}^2 \quad (12)$$

The summation runs over all symmetry species γ and the number $n(\gamma)$ of the nonredundant symmetry coordinates. Unambiguous assignment of the vibrations belonging to the A_{1g} and the T_{1u} symmetry blocks is possible without the aid of normal coordinate analysis. They can therefore be used to generate a good first guess of diagonal symmetry force constants, which in turn serves to estimate the diagonal elements for the E_g and T_{2g} modes according to the relations given in the Appendix. It turns out that the A_{1g} experimental data can be described sufficiently well by (12). For the other symmetries, some off-diagonal elements are needed. They can be determined in a step by step procedure, taking all data into consideration, in which also the f_{ij} are generated. Since the interaction terms f_{Rj} ($j = r, \alpha, \beta$) are very small, they are neglected, leaving us with 15 independent parameters to be determined. The final calculations and refinements, based on (4) and on all experimental data available, result in unambiguous assignment of the fundamentals of H₈Si₈O₁₂, D₈Si₈O₁₂, HD₇Si₈O₁₂, and of the combination bands observed, and they deliver the set of very good force constants in Table 5.

Comparison of the experimental and the theoretical harmonic frequencies ω_j in Table 6 shows very good agreement. Harmonic correction of the experimental Si-H stretching frequencies ν_j has been made according to ref 31. A useful and generally accepted interpretation of the fundamental vibrations in terms of symmetry coordinates can be obtained by applying the potential energy distribution (PED) formula:³²

$$P_{ij} = 100 \left(\frac{\mathcal{F}_{ii} L_{ij}^2}{\sum_k \mathcal{F}_{kk} L_{kj}^2} \right) \% \quad (13)$$

with the L matrix defined by $S = LQ$ whereby Q is the normal coordinates. A certain symmetry coordinate S_i can always be interpreted as stretching $\nu(\text{Si-H})$, $\nu(\text{Si-O})$ or as bending $\delta(\text{O-Si-H})$, $\delta(\text{O-Si-O})$ or $\delta(\text{Si-O-Si})$ movement, symmetric (s) or antisymmetric (as), see also Table 2 in ref 6. Because of $S = LQ$, however, mixing of different types of ν and δ movements is often observed according to $Q_i = \sum a_{ij} S_j$. Fortunately, one of the a_{ij} coefficients is in most cases significantly larger than the others, so the type of vibration according to ν and δ movements still makes sense. The two rightmost columns of Table 6 are based on this rule. It is not astonishing that the totally symmetric modes

do not mix and therefore belong to pure $\nu(\text{Si-H})$, $\delta_s(\text{O-Si-O})$, and $\nu_s(\text{Si-O-Si})$ movements. The same is true for the low-energy E_g mode ω_8 in which each of two opposite Si-O-Si angles change in the same way according to $1/\sqrt{8}(\Phi_1 - \Phi_2 + \Phi_3 - \Phi_4 + \Phi_9 - \Phi_{10} + \Phi_{11} - \Phi_{12})$. This 84-cm⁻¹ vibration reflects the smoothness of the Si-O-Si angle, very nicely illustrated in the large amplitude of the oxygen observed in recent X-ray studies of $\text{H}_8\text{Si}_8\text{O}_{12}$,⁴ of $\text{H}_{10}\text{Si}_{10}\text{O}_{15}$,³³ and of $\text{Co}(\text{CO})_4\text{H}_7\text{Si}_8\text{O}_{12}$.³⁴ We note that the E_g normal modes ω_5 and ω_6 change their type from $\delta_s(\text{O-Si-H})$ and $\nu_s(\text{Si-O-Si})$ for $\text{H}_8\text{Si}_8\text{O}_{12}$ to $\nu_s(\text{Si-O-Si})$ and $\delta_s(\text{O-Si-D})$ for $\text{D}_8\text{Si}_8\text{O}_{12}$. This change also affects the change in polarizability of these modes.

Regarding the symmetry species T_{2g} and T_{1u} , we observe in both cases that the two highest energy modes are pure $\nu(\text{Si-H})$ and $\nu_{as}(\text{Si-O-Si})$ movements, while the lower frequency modes show an increasing coupling of internal vibrations from $\text{H}_8\text{Si}_8\text{O}_{12}$ to $\text{D}_8\text{Si}_8\text{O}_{12}$. This is caused by the shift of ω_{14} and ω_{26} toward the lower energy levels, which favors mode interactions. In the case of ω_{15} it is so strong that $\nu_s(\text{Si-O-Si})$ changes to $\delta_s(\text{O-Si-D})$.

It is now time to examine the results in Tables 6 and 7 and to discuss relations to group frequencies of comparable silicon compounds. Smith³⁵ reported group frequencies for Si-H in the region of $\nu(\text{Si-H}) = 2260\text{--}2100$ cm⁻¹ and $\delta(\text{O-Si-H}) = 960\text{--}800$ cm⁻¹. This fits nicely with $\nu(\text{Si-H}) = 2302, 2291, \text{ and } 2277$ cm⁻¹ and with $\delta(\text{O-Si-H}) = 890$ and 881 cm⁻¹ for $\text{H}_8\text{Si}_8\text{O}_{12}$. The Si-O-Si group shows a characteristic frequency in the region 1130–1000 cm⁻¹. This strong absorption is attributed to the antisymmetric Si-O-Si stretching vibration, which is in accordance with $\nu_{as}(\text{Si-O-Si}) = 1141$ and 1117 cm⁻¹ for $\text{H}_8\text{Si}_8\text{O}_{12}$. The symmetric Si-O-Si stretching vibrations are expected in the region 625–480 cm⁻¹.³⁶ The $\nu_s(\text{Si-O-Si}) = 456$ cm⁻¹ of $\text{H}_8\text{Si}_8\text{O}_{12}$ is at the lower end of this region. Unfortunately, no comparison of $\delta(\text{O-Si-O})$ and $\delta(\text{Si-O-Si})$ with literature data can be made. This is due not only to the fact that these vibrations appear to be less characteristic but also because not sufficiently detailed literature data are available.

The set of internal force constants in Table 5 can be used to calculate the vibrational frequencies for all inactive fundamentals of $\text{H}_8\text{Si}_8\text{O}_{12}$ and $\text{D}_8\text{Si}_8\text{O}_{12}$ collected in Table 7. This means that we have now a complete picture of the vibrational structure of these molecules. The analysis of the potential energy distribution shows that almost all of these fundamentals can be described as localized internal vibrations except the normal modes ω_{30} , ω_{31} , and ω_{32} , which show a slight coupling of internal motions. Visual representation of normal modes on a computer screen can be obtained by means of the atomic displacement matrix A , eq 14,³⁷ fed into an appropriate computer program such as MOBY³⁸ or others:

$$A = M^{-1}B^T(L^{-1})^T \quad (14)$$

Discussion. We have already explained that the spectra of $\text{H}_8\text{Si}_8\text{O}_{12}$ and $\text{D}_8\text{Si}_8\text{O}_{12}$ show some extra bands which do not belong to O_h symmetry fundamentals. We are, however, in the fortunate situation that all this additional information can be understood which has therefore been added to the Tables 2 and 3. Some of it needs further explanation, which is now given.

Nonredundant Symmetry Coordinates. In order to keep the same concept of group frequencies used by other authors,^{28,29,35} the $\delta(\text{O-Si-H})$ type modes are expected in the region 800–1000 cm⁻¹. Furthermore there is no experimental indication for a totally symmetric fundamental mode in this region, and the totally symmetric vibrations observed at 580 cm⁻¹ ($\text{H}_8\text{Si}_8\text{O}_{12}$) and 579 cm⁻¹ ($\text{D}_8\text{Si}_8\text{O}_{12}$) should be described as $\delta(\text{O-Si-O})$. We have therefore exchanged the coordinates S_3 and S_{20} used in our earlier studies⁶ for S_{R1} and S_{R10} , respectively.

Lines Arising due to Solid-State Effects. The FT-Raman spectra of $\text{H}_8\text{Si}_8\text{O}_{12}$ and $\text{D}_8\text{Si}_8\text{O}_{12}$ have been measured as

crystalline powders. Due to symmetry lowering from O_h to T_h , the inactive fundamentals of the symmetry species A_{2g} and T_{1g} can become Raman active. According to the calculated frequencies in Table 7 we assign the lines at 352 and 61 cm⁻¹ to the symmetry species T_{1g} and A_{2g} , respectively. The 61-cm⁻¹ line allows one to estimate the value of f_r . The splitting of the T_{2g} $\nu(\text{Si-H})$ and $\delta(\text{O-Si-H})$ vibrations caused by the S_6 environment of the H atoms in the solid state has already been discussed.

Combination Bands. Correct assignment demands analysis of all symmetry-allowed binary combination and difference bands, which has been carried out by us. It is obvious that low-frequency modes play the most important role in this analysis. Already Lazarev has shown that in many cases the wings of the antisymmetric and the symmetric Si-O-Si stretching modes have to be interpreted as combination and as difference bands, respectively, with a low-frequency $\delta(\text{Si-O-Si})$ movement.³⁹ The mode which adds in our case to the infrared-active ν_{25} $\nu_{as}(\text{Si-O-Si})$ and ν_{28} $\nu_s(\text{Si-O-Si})$ is the E_g Raman line at 84 cm⁻¹, namely, ν_8 . This leads to the infrared-active combination and difference bands $\nu_{25} \pm \nu_8$ at 1215 and 1071 cm⁻¹, respectively, and to the $\nu_{28} + \nu_8$ and $\nu_{27} - \nu_8$ bands at 537 and 490 cm⁻¹, respectively. The 84-cm⁻¹ $\delta(\text{Si-O-Si})$ vibration also mixes into the ν_2 , ν_6 , ν_7 , and ν_{13} Raman modes, which leads to the corresponding extra lines reported in Table 3. Interestingly, the inactive ω_{33} $\delta(\text{Si-O-Si})$ has been found to mix into ν_{26} , which leads to the Raman active line at 811 cm⁻¹ for $\text{H}_8\text{Si}_8\text{O}_{12}$ and at 610 cm⁻¹ in the case of $\text{D}_8\text{Si}_8\text{O}_{12}$.

Bands Arising from $\text{HD}_7\text{Si}_8\text{O}_{12}$. Some of the weak extra bands between 600 and 900 cm⁻¹ observed in the spectrum of $\text{D}_8\text{Si}_8\text{O}_{12}$ belong to $\text{HD}_7\text{Si}_8\text{O}_{12}$ molecules. This is supported by the weak IR absorption at 881 cm⁻¹ which belongs to an O-Si-H bending vibration. Also, the corresponding FT-Raman spectrum shows two weak lines at 2301 and 2292 cm⁻¹ belonging to Si-H stretching modes, and the spectra of two differently deuterated samples show an increase in intensities of these lines for the less completely deuterated sample. Calculation of the fundamental frequencies of the isotopic molecule $\text{HD}_7\text{Si}_8\text{O}_{12}$ with the refined force field for $\text{H}_8\text{Si}_8\text{O}_{12}$ is in agreement with the assignment of the six extra bands in the IR spectrum and five extra lines in the FT-Raman spectrum reported in the Tables 2 and 3.

Low-Frequency Mode at 84 cm⁻¹. This line, which is delicate to measure because of its closeness to the 85-cm⁻¹ Nd:YAG interference, is especially efficient in generating combination and difference bands with IR- and Raman-active Si-O-Si stretching modes. The same $\delta(\text{Si-O-Si})$ vibration appears in the Raman spectrum of $O_h\text{-(CH}_3)_8\text{Si}_8\text{O}_{12}$ at 66 cm⁻¹. If calculated with the $\text{H}_8\text{Si}_8\text{O}_{12}$ force field, we obtain 69 cm⁻¹. This means that the shift from 84 to 66 cm⁻¹ is mainly caused by the larger mass of CH_3 with respect to H.

Missing Raman Line at 820 cm⁻¹ in $\text{D}_8\text{Si}_8\text{O}_{12}$. We have already stated that the fundamental ν_5 has not been observed in $\text{D}_8\text{Si}_8\text{O}_{12}$. Similar observations have been made in the Raman spectra of DSiCl_3 , DSiBr_3 ,⁴⁰ and $\text{DSi}(\text{CH}_3)_3$.⁴¹ We have already observed that the two E_g modes ν_5 and ν_6 show strong coupling of internal motions, and we suspect that this intermolecular interaction influences the change of polarizability to an extent that the ν_5 of $\text{D}_8\text{Si}_8\text{O}_{12}$ scattering becomes too weak to be observed in our experiments. A normal coordinate treatment of HSiCl_3 and DSiCl_3 has revealed a similar result.⁴²

Harmonic Force Field. The force constant $f_{r\beta} - f'_{r\beta}$ cannot be determined unambiguously by the criterion of the root mean square error between the calculated and experimental frequencies only. We have therefore included the relative intensities of the infrared bands as an additional constraint, and we have found that a value of -0.160 mdyn rad⁻¹ shows the best agreement between calculated and experimental relative IR intensities.

TABLE 6: IR- and Raman-Active Fundamentals of $H_8Si_8O_{12}$ and $D_8Si_8O_{12}$

normal mode	experimental (cm ⁻¹)		calculated (cm ⁻¹)		potential energy distribution (%)		type of vibration	
	$H_8Si_8O_{12}$	$D_8Si_8O_{12}$	$H_8Si_8O_{12}$	$D_8Si_8O_{12}$	$H_8Si_8O_{12}$	$D_8Si_8O_{12}$	$H_8Si_8O_{12}$	$D_8Si_8O_{12}$
A_{1g}								
ω ₁	2399	1726	2381	1717	100 S ₁	99 S ₁	ν(Si-H)	ν(Si-D)
ω ₂	580	579	576	570	100 S ₃	100 S ₃	δ _s (O-Si-O)	δ _s (O-Si-O)
ω ₃	456	452	446	442	99 S ₂	99 S ₂	ν _s (Si-O-Si)	ν _s (Si-O-Si)
E_g								
ω ₅	932	820 ^a	922	819	76 S ₆ + 21 S ₅	60 S ₅ + 32 S ₆	δ _s (O-Si-H)	ν _s (Si-O-Si)
ω ₆	697	562	691	560	62 S ₅ + 23 S ₆ + 14 S ₇	70 S ₆ + 16 S ₅ + 14 S ₇	ν _s (Si-O-Si)	δ _s (O-Si-D)
ω ₇	423	422	423	419	78 S ₇ + 20 S ₅	74 S ₇ + 23 S ₅	δ _s (O-Si-O)	δ _s (O-Si-O)
ω ₈	84	84	83	82	96 S ₈	96 S ₈	δ(Si-O-Si)	δ(Si-O-Si)
T_{2g}								
ω ₁₂	2368	1704	2381	1718	100 S ₁₂	99 S ₁₂	ν(Si-H)	ν(Si-D)
ω ₁₃	1117	1115	1116	1113	92 S ₁₄	92 S ₁₄	ν _{as} (Si-O-Si)	ν _{as} (Si-O-Si)
ω ₁₄	890	721	894	737	90 S ₁₅ + 10 S ₁₃	50 S ₁₅ + 44 S ₁₃	δ _s (O-Si-H)	δ _s (O-Si-D)
ω ₁₅	610	541	613	542	69 S ₁₃ + 16 S ₁₇ + 12 S ₁₅	49 S ₁₅ + 28 S ₁₃ + 22 S ₁₇	ν _s (Si-O-Si)	δ _s (O-Si-D)
ω ₁₆	414	405	418	402	80 S ₁₇	78 S ₁₇ + 14 S ₁₃	δ _{as} (O-Si-O)	δ _{as} (O-Si-O)
ω ₁₇	171	170	168	166	71 S ₁₆ + 24 S ₁₇	71 S ₁₆ + 23 S ₁₇	δ _s (O-Si-O)	δ _s (O-Si-O)
T_{1u}								
ω ₂₄	2379	1712	2381	1718	100 S ₂₄	99 S ₂₄	ν(Si-H)	ν(Si-D)
ω ₂₅	1141	1140	1143	1141	92 S ₂₆	91 S ₂₆	ν _{as} (Si-O-Si)	ν _{as} (Si-O-Si)
ω ₂₆	881	687	881	691	93 S ₂₇	66 S ₂₇ + 23 S ₂₅	δ _{as} (O-Si-H)	δ _{as} (O-Si-D)
ω ₂₇	566	531	569	546	56 S ₂₉ + 42 S ₂₅	73 S ₂₉ + 18 S ₂₅	δ _{as} (O-Si-O)	δ _{as} (O-Si-O)
ω ₂₈	465	457	481	453	45 S ₂₅ + 21 S ₂₈ + 17 S ₂₉	52 S ₂₅ + 28 S ₂₇ + 13 S ₂₉	ν _s (Si-O-Si)	ν _s (Si-O-Si)
ω ₂₉	399	392	397	393	57 S ₂₈ + 30 S ₂₉	59 S ₂₈ + 26 S ₂₉	δ _s (O-Si-O)	δ _s (O-Si-O)

^a Calculated from the product rule.**TABLE 7: Inactive Fundamentals of $H_8Si_8O_{12}$ and $D_8Si_8O_{12}$**

normal mode	calculated (cm ⁻¹)		potential energy distribution (%)		type of vibration	
	$H_8Si_8O_{12}$	$D_8Si_8O_{12}$	$H_8Si_8O_{12}$	$D_8Si_8O_{12}$	$H_8Si_8O_{12}$	$D_8Si_8O_{12}$
A_{2g}						
ω ₄	57	57	100 S ₄	100 S ₄	τ _{as} (Si-O-Si)	τ _{as} (Si-O-Si)
T_{1g}						
ω ₉	1161	1160	97 S ₉	97 S ₉	ν _{as} (Si-O-Si)	ν _{as} (Si-O-Si)
ω ₁₀	865	639	99 S ₁₀	96 S ₁₀	δ _{as} (O-Si-H)	δ _{as} (O-Si-D)
ω ₁₁	356	348	90 S ₁₁	85 S ₁₁	δ _{as} (O-Si-O)	δ _{as} (O-Si-O)
A_{2u}						
ω ₁₈	2381	1718	100 S ₁₈	99 S ₁₈	ν(Si-H)	ν(Si-D)
ω ₁₉	1082	1077	95 S ₁₉	94 S ₁₉	ν _{as} (Si-O-Si)	ν _{as} (Si-O-Si)
ω ₂₀	304	299	94 S ₂₀	94 S ₂₀	δ _{as} (O-Si-O)	δ _{as} (O-Si-O)
E_u						
ω ₂₁	1158	1158	98 S ₂₁	98 S ₂₁	ν _{as} (Si-O-Si)	ν _{as} (Si-O-Si)
ω ₂₂	862	633	99 S ₂₂	99 S ₂₂	δ _{as} (O-Si-H)	δ _{as} (O-Si-D)
ω ₂₃	166	160	92 S ₂₃	90 S ₂₃	δ _{as} (O-Si-O)	δ _{as} (O-Si-O)
T_{2u}						
ω ₃₀	918	810	78 S ₃₁ + 21 S ₃₀	61 S ₃₀ + 34 S ₃₁	δ _s (O-Si-H)	ν _s (Si-O-Si)
ω ₃₁	682	554	71 S ₃₀ + 20 S ₃₁	70 S ₃₁ + 24 S ₃₀	ν _s (Si-O-Si)	δ _s (O-Si-D)
ω ₃₂	303	300	81 S ₃₂ + 12 S ₃₀	81 S ₃₂ + 13 S ₃₀	δ _s (O-Si-O)	δ _s (O-Si-O)
ω ₃₃	68	68	92 S ₃₃	92 S ₃₃	δ(Si-O-Si)	δ(Si-O-Si)

IV. Correlation O_h - $H_8Si_8O_{12} \rightarrow O_h$ - $(-O)_8Si_8O_{12} \rightarrow D_{4h}$ - $(-O)_8Si_8O_{12}$

We have succeeded in obtaining a good harmonic force field for $H_8Si_8O_{12}$ in terms of internal force constants, and we now show how the information gained can be used to describe the vibrational structure of zeolite A. The first step is to transform the $H_8Si_8O_{12}$ molecule into the O_h - $(-O)_8Si_8O_{12}$ fragment by substitution of the hydrogen atoms by oxygen. The lengths of the eight new Si-O bonds are taken equal to those of $H_8Si_8O_{12}$. The necessary adaptation of the definitions of the force field in Table 1 is straightforward. We exchange all subscripts R and α by r and β , respectively, and we add a prime according to the rules given in this table. This leads to a force field of nine different internal force constants, eight of them the same as those in Table 5. It suggests itself to set the unknown $f_{\beta\beta} - f'_{\beta\beta}$ equal to $f_{\alpha\beta} - f'_{\alpha\beta}$. The force field obtained in this manner can be used to perform a normal coordinate analysis of O_h - $(-O)_8Si_8O_{12}$ in terms of the same internal symmetry coordinates as those of O_h - $H_8Si_8O_{12}$.⁶ This allows one to generate a full correlation diagram for the fundamentals of $H_8Si_8O_{12}$ and the fragment, according to the PED analysis which is shown in Figure 3 for the IR and for the Raman active modes. Let us remark that Figure 3 should not

be mixed up with quantum mechanical correlation diagrams in which states of the same symmetry are not allowed to cross. In vibrational spectroscopy the idea behind these diagrams is to connect vibrations of the same character, e.g., $\nu_{as}(\text{Si-O-Si})$ in $H_8Si_8O_{12}$ with $\nu_{as}(\text{Si-O-Si})$ in $(-O)_8Si_8O_{12}$ and so on. It corresponds to the frequently and successfully used approach of group frequencies. Nevertheless, the small influence of the O_h to D_{4h} symmetry lowering allows one to preserve the character of the vibrations as well as the symmetry for the step from O_h - $(-O)_8Si_8O_{12}$ to D_{4h} - $(-O)_8Si_8O_{12}$.

Three different Si-O bond lengths, four different O-Si-O angles, and two different Si-O-Si angles have been observed in X-ray studies of zeolite A.⁴³ These data have been used to generate the D_{4h} - $(-O)_8Si_8O_{12}$ fragment on which a normal coordinate analysis has been performed. The main results of this analysis are again illustrated in the correlation diagram in Figure 3. An important consequence of the symmetry lowering is the splitting of all IR-active T_{1u} modes into $E_u + A_{2u}$ and of all Raman-active E_g and T_{2g} modes into $A_{1g} + B_{1g}$ and $B_{2g} + E_g$, respectively, according to Table 8. In addition to this, the inactive T_{2u} modes in O_h symmetry split into an inactive B_{2u} and an IR-active E_u species. The same occurs for the inactive T_{1g} modes, which split

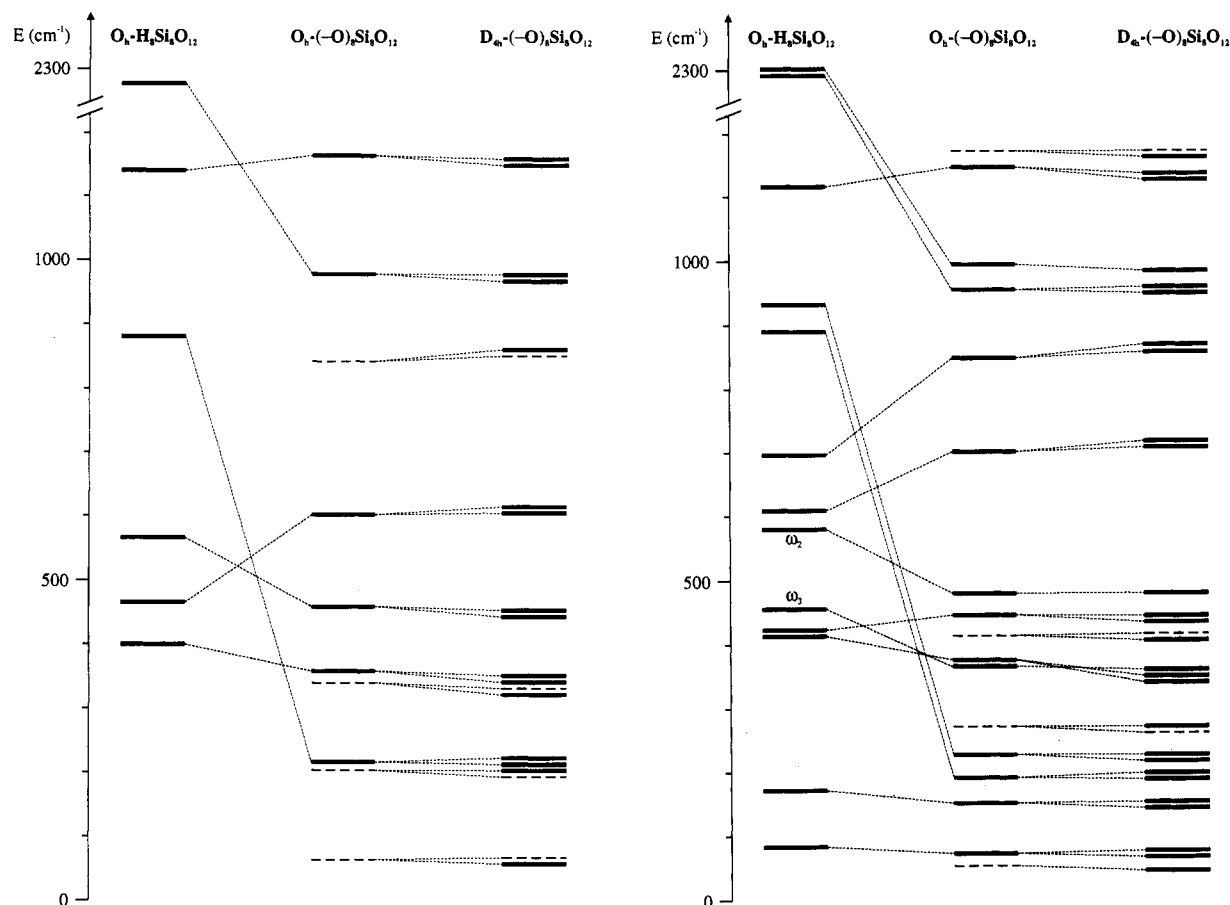


Figure 3. Correlation diagrams of the fundamentals of $O_h\text{-H}_8\text{Si}_8\text{O}_{12}$, $O_h\text{-}(-\text{O})_8\text{Si}_8\text{O}_{12}$, and $D_{4h}\text{-}(-\text{O})_8\text{Si}_8\text{O}_{12}$. Left: IR-active normal modes. Right: Raman-active normal modes. Thin, dashed lines are inactive fundamentals.

TABLE 8: Correlation Table for the Point Groups O_h , D_{4h} , and D_{2d}

O_h	D_{4h}	D_{2d}
$A_{1g}(\text{R})$	$A_{1g}(\text{R})$	$A_1(\text{R})$
$A_{2g}(\text{in})$	$B_{1g}(\text{R})$	$B_1(\text{R})$
$E_g(\text{R})$	$A_{1g}(\text{R}) + B_{1g}(\text{R})$	$A_1(\text{R}) + B_1(\text{R})$
$T_{1g}(\text{in})$	$A_{2g}(\text{in}) + E_g(\text{R})$	$A_2(\text{in}) + E(\text{IR,R})$
$T_{2g}(\text{R})$	$B_{2g}(\text{R}) + E_g(\text{R})$	$B_2(\text{IR,R}) + E(\text{IR,R})$
$A_{1u}(\text{in})$	$A_{1u}(\text{in})$	$B_1(\text{R})$
$A_{2u}(\text{in})$	$B_{1u}(\text{in})$	$A_1(\text{R})$
$E_u(\text{in})$	$A_{1u}(\text{in}) + B_{1u}(\text{in})$	$B_1(\text{R}) + A_1(\text{R})$
$T_{1u}(\text{IR})$	$A_{2u}(\text{IR}) + E_u(\text{IR})$	$B_2(\text{IR,R}) + E(\text{IR,R})$
$T_{2u}(\text{in})$	$B_{2u}(\text{in}) + E_u(\text{IR})$	$A_2(\text{in}) + E(\text{IR,R})$

into the inactive A_{2g} and the Raman-active E_g species. Furthermore the inactive A_{2g} mode in O_h symmetry becomes Raman active. The PED analysis reveals assignment of four energy regions to characteristic vibrations. All fundamentals between 1200 and 1100 cm^{-1} are characteristic antisymmetric Si–O–Si stretching modes. The 1000–900- cm^{-1} region contains only characteristic stretching vibrations of the terminal Si–O bonds. The symmetric Si–O–Si stretchings fall between 900 and 750 cm^{-1} . Below 100 cm^{-1} pure Si–O–Si bending or torsion is observed. All other vibrations appear in the 750–100- cm^{-1} region. Most of them are admixtures of symmetric Si–O–Si stretching and O–Si–O bending movements and can therefore be regarded as noncharacteristic. Nevertheless, there are some vibrations between 500 and 100 cm^{-1} which can be described as characteristic O–Si–O or terminal O–Si–O bending modes.

Since the distortion of the geometry from O_h to D_{4h} symmetry is small, the results of the potential energy distribution for both molecules differ by only a few percent with two interesting exceptions, the totally symmetric vibrations ω_2 and ω_3 according to Figure 3. For them a small change in bond lengths and bond angles causes a large change in the potential energy distribution.

In the cubical molecule ω_2 and ω_3 can be considered as being a dominantly O–Si–O bending and symmetric Si–O–Si stretching, respectively. A small distortion of the geometry causes strong coupling, and they become admixtures of each other. We now have a good basis for the next step, which means to proceed to the $D_{4h}\text{-}(\equiv\text{SiO})_8\text{Si}_8\text{O}_{12}$ framework and from there to zeolite A. Before doing so, we give some information on the FT-Raman spectra of zeolite A.

V. FT-Raman Spectra of Zeolite A

Raman spectra of zeolite A have been reported by several authors, and selected data are given in Table 9, in comparison to our own measurements. While classical Raman spectroscopy on zeolites is not easy to perform because of the small scattering cross section, luminescence problems, and stability of the samples, the possibilities opened by the NIR FT technique are promising. In fact, no further pretreatment of the zeolites (e.g., heating, oxygen treatment, and evacuation) was necessary to obtain the data in Figure 4, where the intensity-corrected Raman spectra of Na^+ -exchanged zeolite A, Na-A, and of Ag^+ -exchanged zeolite A, Ag-A, are compared with the spectrum of Na^+ -exchanged zeolite Y, Na-Y. All spectra have been taken at ambient conditions so that weak water bendings appear at 1648 and 1633 cm^{-1} for the zeolites Na-A and Na-Y, respectively, which are not shown in Figure 4, however. The Na-A spectrum, left and right, exhibits 10 well-distinguished bands and a shoulder, starting from 246 up to 1103 cm^{-1} . The 465- cm^{-1} shoulder and the 246- cm^{-1} band have not hitherto been reported. The small peak at 131 cm^{-1} which appears in all three spectra is due to the intensity correction and does not belong to the zeolites.

Our interest on Ag^+ -exchanged zeolites has focused on the photoreaction with water as the reducing agent, whereby molecular oxygen is liberated from water at neutral pH.⁴⁴ In situ IR

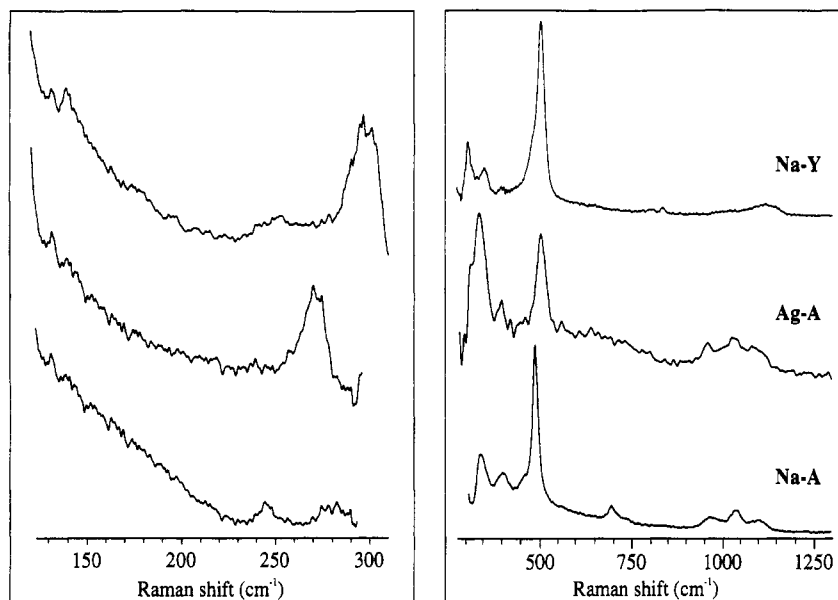


Figure 4. Corrected FT-Raman spectra of zeolites A and Y with a resolution of 4 cm^{-1} . Left: Na-A, 1.1-W laser power, 1000 scans; Ag-A, 800-mW laser power, 100 scans; Na-Y, 630-mW laser power, 1000 scans. Right: Na-A, 670-mW laser power, 2650 scans; Ag-A, 1.2-W laser power, 100 scans and smoothed by a factor of 8; Na-Y, 600-mW laser power, 4800 scans.

TABLE 9: Raman Frequencies (cm^{-1}) of Hydrated Zeolites A with Different Cations

zeolite A	~250	~280	~340	~400	~450	~490	~700	~735	~845	~960	~1000	~1045	~1095	addnl. lines	ref
Li-A		288		383		499		736		940	983		1074	209	54
Li-A			356	381	440	497		730	845	937	996	1059	1084		48
Na-A		280	340	410		490	700			977		1037	1100		12
Na-A			335	405		490	699	738	850	971	1000	1039	1099		48
Na-A	246	280	343	403	465	490	701	736		971		1041	1103		this work
K-A			331	405		487	694	735	840	960	998	1030	1095		48
Tl-A			333	400		482		738	840	952		1030	1084	665	48
Ag-A		270	334	394		502				962		1030	1090		this work

transmission spectroscopy on thin self-supporting zeolite wafers has been shown to be useful for studying such systems,⁴⁵ and Raman experiments have the potential for extending the range of applicability of vibrational studies. The great advantage of the FT-Raman technique with excitation in the near infrared is that no photochemical reaction is induced. Black body radiation caused by heating the zeolite sample is the remaining problem. Nevertheless, reasonable results could be obtained as we report in Figure 4 the first Ag-A Raman spectrum published so far. The 246-, 465-, 701-, and 736- cm^{-1} bands of Na-A could not be traced with certainty in this spectrum, and all maxima are shifted by about 10 cm^{-1} to lower energies with the exception of the most prominent band, which goes upward by 12 cm^{-1} ! Noticeable intensity enhancement is observed at 270 and 334 cm^{-1} . To get a better feeling of the significance of these results, it is useful to compare them with the spectrum of Na-Y, taken under the same conditions. The 10 bands at 139, 250, 300, 348, 392, 503, 803, 836, 1025, and 1116 cm^{-1} and a shoulder at 480 cm^{-1} are readily recognized and in agreement with data reported in the literature.^{12,46,47}

Returning to Table 9, good agreement between our Na-A and the literature Na-A data is observed. High sensitivity of our instrumentation and the wide spectral range covered by the filters have allowed one to measure the two additional frequencies at 246 and 465 cm^{-1} . The nature of the 850- cm^{-1} and the 1000- cm^{-1} bands reported by Dutta et al.⁴⁸ will be explained later. The same authors have also discussed the influence of the cations on the Raman spectra of zeolite A.

VI. Correlation between $\text{H}_8\text{Si}_8\text{O}_{12}$ and Zeolite A

In order to describe the vibrational structure of zeolites, we have to overcome two major problems. The first one is the choice

of an appropriate model for a reliable description of such an extended system. Because the structure of a zeolite A can be built with the double four ring (D_{4h}^1), the molecular fragment $\text{D}_{4h}^-(\text{O})_8\text{Si}_8\text{O}_{12}$ appears as a possible model, as discussed in section IV. This fragment is, however, still insufficient because it cannot describe the vibrations involving the terminal oxygen atoms in a correct way. It can fortunately be extended easily to the $\text{D}_{4h}^-(\equiv\text{SiO})_8\text{Si}_8\text{O}_{12}$ by adding eight silicon atoms in order to have all oxygen atoms as bridges. The important change is that this adds eight Si-O stretching modes and transforms the terminal $\nu(\text{Si-O})$ stretchings into symmetric and antisymmetric $\nu(\text{Si-O-Si})$ vibrations. It also adds eight $\delta(\text{Si-O-Si})$ which are, however, of less importance.

The second problem is the choice of a good harmonic force field. The purpose of the first part of this paper was to obtain good force constants in terms of internal coordinates for the molecule $\text{H}_8\text{Si}_8\text{O}_{12}$. These force constants can be transferred to the fragment $\text{D}_{4h}^-(\equiv\text{SiO})_8\text{Si}_8\text{O}_{12}$, as discussed in section IV. This fragment would be an excellent model for a zeolite A with a high Si/Al ratio. Because zeolite A consists of silicon and aluminum atoms in equal ratio, it is necessary to substitute half of the Si by Al, according to Löwenstein's rule. This leads to the fragment $\text{D}_{2d}^-(\equiv\text{TO})_8\text{T}_8\text{O}_{12}$, T = Si or Al and Si/Al = 1, which has turned out to be sufficient. The calculation of the frequencies of these two fragments was performed with the same force field as used for the fragment $\text{D}_{4h}^-(\text{O})_8\text{Si}_8\text{O}_{12}$ with three exceptions. The force constant $f_{\beta\beta} - f'_{\beta\beta}$, which could not be determined in the force field of $\text{H}_8\text{Si}_8\text{O}_{12}$, was set equal to 0.328 $\text{mdyn } \text{\AA} \text{ rad}^{-2}$ as reported in ref 49. Furthermore we have adjusted $f_{\beta} - f_{\beta\beta}$ to a value of 1.12 $\text{mdyn } \text{\AA} \text{ rad}^{-2}$ in order to match the strong zeolite A Raman band at 490 cm^{-1} (see Figure 6). The Al-O stretching force constant was estimated as 3.26 $\text{mdyn } \text{\AA}^{-1}$ by scaling the

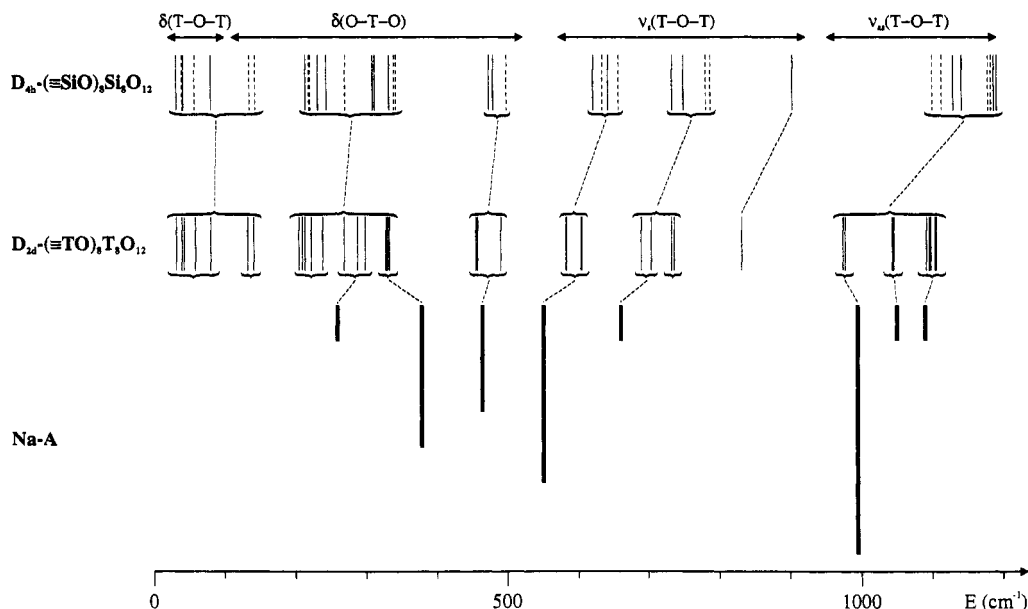


Figure 5. Correlation of IR-active fundamentals of $D_{4h}-(\equiv\text{SiO})_8\text{Si}_8\text{O}_{12}$ and $D_{2d}-(\equiv\text{TO})_8\text{T}_8\text{O}_{12}$ and the relation to the literature IR spectrum of zeolite Na-A.¹¹ The dashed lines are inactive fundamentals of $D_{4h}-(\equiv\text{SiO})_8\text{Si}_8\text{O}_{12}$ which become IR-active in $D_{2d}-(\equiv\text{TO})_8\text{T}_8\text{O}_{12}$.

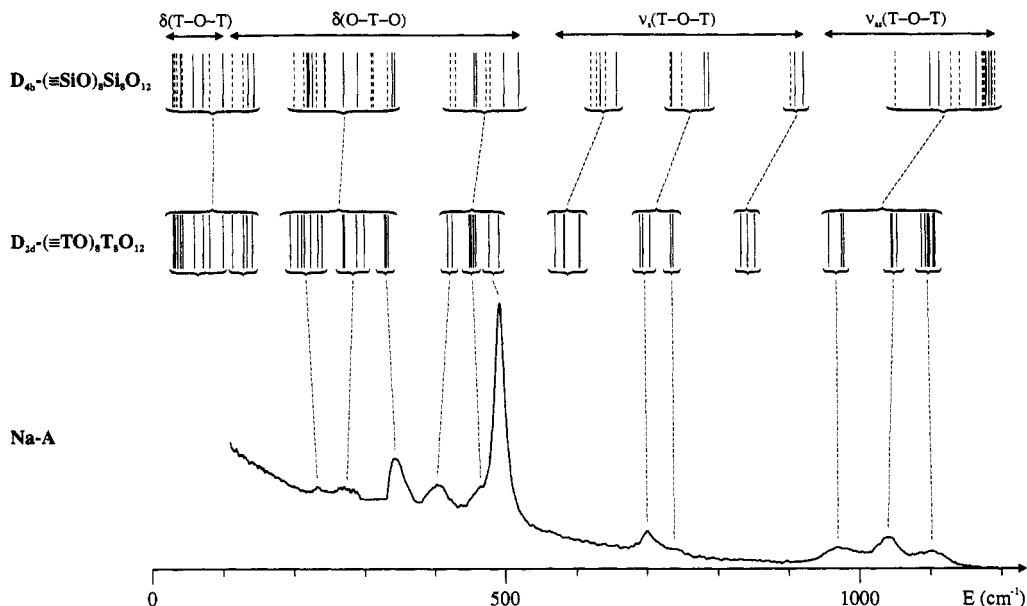


Figure 6. Correlation of Raman-active fundamentals of $D_{4h}-(\equiv\text{SiO})_8\text{Si}_8\text{O}_{12}$ and $D_{2d}-(\equiv\text{TO})_8\text{T}_8\text{O}_{12}$ and the relation to the FT-Raman spectrum of zeolite Na-A as measured by us. The dashed lines are inactive fundamentals of $D_{4h}-(\equiv\text{SiO})_8\text{Si}_8\text{O}_{12}$ which become Raman active in $D_{2d}-(\equiv\text{TO})_8\text{T}_8\text{O}_{12}$.

Si-O value with the ratio of the corresponding force constants $f_r(\text{Al-O})/f_r(\text{Si-O}) = 0.639$ obtained from ref 49.

In Figures 5 and 6, we report a correlation between the calculated IR and Raman frequencies of $D_{4h}-(\equiv\text{SiO})_8\text{Si}_8\text{O}_{12}$, $D_{2d}-(\equiv\text{TO})_8\text{T}_8\text{O}_{12}$, and the experimental spectra of zeolite A. From these figures it is evident that the line spectra show seven distinct groups of frequencies, indicated with horizontal brackets and connected by dashed lines. The correlation shows a growing dependence of the frequencies on the Si/Al ratio with increasing frequencies, which is due to the augmenting T-O stretching contribution. We now focus on a detailed description of the IR- and Raman-active fundamentals of the fragment $D_{2d}-(\equiv\text{TO})_8\text{T}_8\text{O}_{12}$ based on the results of the PED analysis reported in Table 10. The assignment of the type of vibration was facilitated by the inspection of each mode on the computer screen with MOBY.^{38,50}

Vibrations of Zeolite A. It is remarkable that the IR and Raman spectra of $D_{2d}-(\equiv\text{TO})_8\text{T}_8\text{O}_{12}$ can be divided into four main regions, denoted by $\nu_{as}(\text{T-O-T})$, $\nu_s(\text{T-O-T})$, $\delta(\text{O-T-O})$, and $\delta(\text{T-O-T})$ with the exception of four lines which will be

discussed later. Let us add that we do not discuss the vibrations belonging to the charge-compensating cations which appear below 300 cm^{-1} .⁴⁵ We will concentrate on the zeolite framework.

Region 1110–950 cm^{-1} . All fundamentals in this region can be described as characteristic antisymmetric T-O-T stretching vibrations. This region can be further divided into three subgroups as evident from Table 10 and illustrated in Figures 5 and 6. These groups can be assigned to the three bands of the IR as well as of the Raman spectra of zeolite Na-A. Dutta et al.⁵¹ have interpreted the three well-defined bands in the Na-A Raman spectrum at 971, 1041, and 1103 cm^{-1} as localized stretching vibrations of the three different oxygen atoms in zeolite A, T-O(3), T-O(1), and T-O(2), respectively. The labeling of the T-O(1), T-O(2), and T-O(3) is explained in ref 52. Our PED analysis shows, however, that only the frequency at 1041 cm^{-1} can be described as a localized mode, namely, $\nu_{as}(\text{T-O}(2)\text{-T})$. The band at 1103 cm^{-1} has to be understood as a mixture of different vibrations, each of them dominantly characterized by a certain oxygen site, whereas all oxygen sites mix into the modes which form the 971- cm^{-1} band.

TABLE 10: Fundamentals of $D_{2d}(\equiv\text{TO})_8\text{T}_8\text{O}_{12}$

symmetry	calcd (cm^{-1})	potential energy distribution (%)									type of vibration
		Si-O(1)	Si-O(2)	Si-O(3)	Al-O(1)	Al-O(2)	Al-O(3)	O-Si-O	O-Al-O	Si-O-Al	
B ₂ (IR,R)	1106	49	9	13	12	6	2	6	3	0	$\nu_{\text{as}}(\text{T-O}(1)-\text{T})$
E(IR,R)	1104	18	4	51	4	4	11	5	3	0	$\nu_{\text{as}}(\text{T-O}(3)-\text{T})$
E(IR,R)	1098	12	47	10	5	15	5	6	0	0	$\nu_{\text{as}}(\text{T-O}(2)-\text{T})$
A ₁ (R)	1096	18	52	2	5	17	1	5	0	0	$\nu_{\text{as}}(\text{T-O}(2)-\text{T})$
B ₂ (IR,R)	1096	0	48	23	0	15	8	5	1	0	$\nu_{\text{as}}(\text{T-O}(2)-\text{T})$
A ₂ (in)	1092	0	0	72	0	0	22	5	1	0	$\nu_{\text{as}}(\text{T-O}(3)-\text{T})$
E(IR,R)	1092	20	6	45	6	2	15	5	1	0	$\nu_{\text{as}}(\text{T-O}(3)-\text{T})$
A ₁ (R)	1087	35	5	34	9	1	10	5	1	0	$\nu_{\text{as}}(\text{T-O}(1,3)-\text{T})$
B ₁ (R)	1087	0	0	73	0	0	22	5	0	0	$\nu_{\text{as}}(\text{T-O}(3)-\text{T})$
A ₁ (R)	1052	0	59	1	1	36	1	0	2	0	$\nu_{\text{as}}(\text{T-O}(2)-\text{T})$
E(IR,R)	1046	1	60	4	0	32	1	1	1	0	$\nu_{\text{as}}(\text{T-O}(2)-\text{T})$
B ₂ (IR,R)	1044	4	60	2	0	32	0	1	1	0	$\nu_{\text{as}}(\text{T-O}(2)-\text{T})$
B ₂ (IR,R)	977	8	14	17	20	12	24	1	4	0	$\nu_{\text{as}}(\text{T-O}-\text{T})$
E(IR,R)	974	12	15	14	14	12	28	1	4	0	$\nu_{\text{as}}(\text{T-O}-\text{T})$
A ₁ (R)	956	16	18	24	9	12	17	0	4	0	$\nu_{\text{as}}(\text{T-O}-\text{T})$
A ₁ (R)	851	4	0	3	37	0	18	12	25	1	$\nu_3(\text{T-O}(1,3)-\text{T})$
B ₁ (R)	841	0	0	7	0	0	54	13	25	1	$\nu_3(\text{T-O}(3)-\text{T})$
E(IR,R)	831	5	0	5	28	0	28	10	23	1	$\nu_3(\text{T-O}(1,3)-\text{T})$
A ₂ (in)	823	0	0	11	0	0	55	10	23	1	$\nu_3(\text{T-O}(3)-\text{T})$
E(IR,R)	736	3	5	23	0	9	26	6	27	1	$\nu_3(\text{T-O}(3)-\text{T})$
B ₂ (IR,R)	732	23	2	12	25	6	0	3	28	1	$\nu_3(\text{T-O}(1)-\text{T})$
B ₂ (IR,R)	703	0	20	5	5	24	9	13	23	1	$\nu_3(\text{T-O}(2)-\text{T})$
A ₁ (R)	693	1	20	1	0	34	0	15	26	3	$\nu_3(\text{T-O}(2)-\text{T})$
E(IR,R)	689	6	19	5	5	24	4	10	26	1	$\nu_3(\text{T-O}(2)-\text{T})$
E(IR,R)	605	2	3	9	2	24	14	31	12	3	$\nu_3(\text{T-O}(2,3)-\text{T})$
B ₂ (IR,R)	604	0	12	4	1	41	7	22	11	2	$\nu_3(\text{T-O}(2)-\text{T})$
B ₂ (IR,R)	583	5	3	3	17	14	9	32	14	3	$\nu_3(\text{T-O}-\text{T})$
E(IR,R)	582	1	10	2	5	28	16	24	12	2	$\nu_3(\text{T-O}(2,3)-\text{T})$
A ₁ (R)	570	1	18	6	0	56	1	13	4	1	$\nu_3(\text{T-O}(2)-\text{T})$
E(IR,R)	490	5	0	3	5	0	5	46	34	2	$\delta(\text{O-T-O})$
A ₂ (in)	490	0	0	8	0	0	10	47	35	0	$\delta(\text{O-T-O})$
A ₁ (R)	476	8	9	8	13	15	19	16	10	2	$\nu_3(\text{T-O}-\text{T})$
E(IR,R)	457	3	5	4	10	8	6	32	31	1	$\delta(\text{O-T-O})$
B ₂ (IR,R)	454	0	4	6	0	8	12	36	33	1	$\delta(\text{O-T-O})$
A ₁ (R)	451	3	0	2	2	0	3	45	43	2	$\delta(\text{O-T-O})$
B ₁ (R)	448	0	0	5	0	0	5	45	43	2	$\delta(\text{O-T-O})$
A ₁ (R)	424	2	0	1	9	2	1	44	36	5	$\delta(\text{O-T-O})$
B ₁ (R)	417	0	0	4	0	0	9	49	38	0	$\delta(\text{O-T-O})$
E(IR,R)	333	0	8	0	1	7	0	61	19	4	$\delta(\text{O-T-O})$
A ₂ (in)	330	0	0	0	0	0	1	48	47	4	$\delta(\text{O-T-O})$
E(IR,R)	330	0	4	0	0	9	1	30	52	4	$\delta(\text{O-T-O})$
B ₂ (IR,R)	328	2	13	0	2	17	1	37	20	8	$\delta(\text{O-T-O})$
E(IR,R)	299	0	8	3	0	19	4	22	38	6	$\delta(\text{O-T-O})$
B ₂ (IR,R)	288	0	13	8	1	30	12	10	24	2	$\nu_3(\text{T-O}(2,3)-\text{T})$
A ₁ (R)	271	0	6	15	0	10	26	15	19	9	$\nu_3(\text{T-O}(2,3)-\text{T})$
E(IR,R)	269	0	1	0	0	1	0	45	47	6	$\delta(\text{O-T-O})$
A ₂ (in)	262	0	0	0	0	0	0	49	51	0	$\delta(\text{O-T-O})$
B ₂ (IR,R)	239	0	0	6	0	1	10	30	35	18	$\delta(\text{O-T-O})$
B ₁ (R)	233	0	0	12	0	0	22	29	36	1	$\delta(\text{O-T-O})$
E(IR,R)	223	3	1	8	6	1	16	28	31	6	$\delta(\text{O-T-O})$
A ₂ (in)	215	0	0	15	0	0	28	27	30	0	$\delta(\text{O-T-O})$
A ₁ (R)	214	11	8	0	21	12	1	20	21	6	$\nu_3(\text{T-O}(1,2)-\text{T})$
B ₂ (IR,R)	214	8	1	0	14	2	0	29	28	18	$\delta(\text{O-T-O})$
E(IR,R)	210	0	0	14	0	0	24	34	21	7	$\delta(\text{O-T-O})$
E(IR,R)	205	8	3	4	13	5	6	19	35	7	$\delta(\text{O-T-O})$
A ₁ (R)	194	1	9	2	0	18	3	30	34	3	$\delta(\text{O-T-O})$
B ₂ (IR,R)	141	3	3	1	5	5	2	40	40	1	$\delta(\text{O-T-O})$
E(IR,R)	133	1	3	1	1	4	2	44	44	0	$\delta(\text{O-T-O})$
A ₁ (R)	128	1	1	0	1	1	0	34	34	28	$\delta(\text{O-T-O})$
B ₁ (R)	113	0	0	1	0	0	1	49	49	0	$\delta(\text{O-T-O})$
A ₁ (R)	100	0	0	0	0	0	1	1	2	96	$\delta(\text{T-O-T})$
E(IR,R)	81	1	0	0	2	0	0	4	4	89	$\delta(\text{T-O-T})$
B ₁ (R)	72	0	0	0	0	0	0	2	2	96	$\delta(\text{T-O-T})$
A ₂ (in)	62	0	0	0	0	0	0	3	3	94	$\delta(\text{T-O-T})$
E(IR,R)	59	0	0	1	0	0	1	8	8	82	$\delta(\text{T-O-T})$
B ₂ (IR,R)	43	0	0	2	0	0	2	12	8	76	$\delta(\text{T-O-T})$
B ₂ (IR,R)	40	2	0	0	3	0	0	8	12	75	$\delta(\text{T-O-T})$
A ₁ (R)	36	0	0	0	0	0	0	25	23	52	$\delta(\text{T-O-T})$
E(IR,R)	32	0	0	0	1	0	0	7	7	85	$\delta(\text{T-O-T})$
A ₁ (R)	30	0	0	0	1	0	1	5	7	86	$\delta(\text{T-O-T})$

Regions 860–830, 740–680, and 610–570 cm^{-1} . These regions belong to vibrations which are primarily of symmetric T–O–T stretching character. Table 10 shows that the $\nu(\text{T-O})$ part of the potential energy between 860–830 and 610–570 cm^{-1} is concentrated on the Al. The potential $\nu(\text{T-O})$ energy at 740–680 cm^{-1}

is almost equally divided between Si and Al, and the corresponding vibrations can be divided into two subgroups: the three frequencies 703, 693, and 689 cm^{-1} are located on the O(2) site whereas the remaining two frequencies are located on O(1) and O(3).

Regions 500–410 and 340–190 cm^{-1} . The fundamentals of

TABLE 11: Comparison of Internal Force Constants of D_{4h}(≡SiO)₈Si₈O₁₂ and Similar Silicate Structures (for units see Table 5)

force constant	this work	ref 53 ^a	ref 9 ^b	ref 49 ^c	ref 55 ^d
f_r	5.10	5.94	6.54	4.89	6.00
f_{rr}	0.275	0.843		0.415 ^h	
f'_{rr}	0.153	0.711		0.655	0.228
$f_{\beta}f_{\beta\beta}$	1.12 ^e	0.729	1.06	0.760	1.08
$f_{\beta\beta}f'_{\beta\beta}$	0.328 ^f	0.167		0.305	0.123
$f_{r\beta}f'_{r\beta}$	-0.160	0.263		0.191	0.274
f_{Φ}	0.091	0.126	0.236	0.240 ^h	
$f_{r\Phi}$	0.036	0.398		0.090 ^h	
$f_{\beta\Phi}$	0.0026				
f_r	0.0040 ^g	0.0056	0.118	0.120 ^h	

^a Internal force constants from vibrational normal modes of α and β quartz. ^b Internal force constants from vibrational modes of silicate structures. ^c Internal force constants according to the adjusted valence force field (AVFF) for zeolite Na-X. ^d Internal force constants from quantum chemical calculations for H₄SiO₄. ^e See text. ^f Mean value of the corresponding force constants $f_{\beta\beta}$ - $f'_{\beta\beta}$ of Si and Al from ref 49. ^g Mean value from the 61-cm⁻¹ FT-Raman line due to solid-state effects (see Table 3) and ref 56. ^h Force constants which are related to at least one internal coordinate with an aluminum atom.

these two regions are characteristic $\delta(\text{O-T-O})$ bending modes with the exceptions of the four frequencies at 476, 288, 271, and 214 cm⁻¹, which are primarily of symmetric T-O-T stretching character (see Discussion). These regions can be further divided into subgroups as shown in Figures 5 and 6. Only tentative correlation of these subgroups and the experimental spectra is possible at the present time.

Region 150-20 cm⁻¹. The vibrations of this region may be divided into two subgroups: those above 100 cm⁻¹ which are of characteristic $\delta(\text{O-T-O})$ type and those below this limit which may be considered as being characteristic $\delta(\text{T-O-T})$. Not included in this analysis are the torsional modes which are expected below 100 cm⁻¹.

Discussion. Comparison of Force Fields. Several empirical and theoretical studies have been the subject of determining the vibrational structure of silicates in the past 20 years,^{9,10,13} and we compare in Table 11 our force constants with selected literature values. There is some agreement and some disagreement between these data. Since different molecules and models are compared, small details should be disregarded. Our value of f_r is close to that reported in ref 49, whereas the values of the other authors are much higher. The stretching interaction force constants f_{rr} and f'_{rr} determined by us are, however, significantly smaller than those reported in the literature. The same is true for f_{Φ} while there is remarkable agreement for the $f_{\beta} - f_{\beta\beta}$ values. All interaction force constants have a positive sign with the exception of our $f_{r\beta} - f'_{r\beta}$, which is negative. Finally, our value of $f_{r\Phi}$ is in accordance with that of ref 49, whereas Etchepare et al.⁵³ reported a much higher value.

$\nu_s(\text{T-O-T})$ below 500 cm⁻¹. Four vibrations do not fit into the general scheme as discussed above. They are all of primarily symmetric T-O-T stretching character. Inspection of the 476-cm⁻¹ vibration with MOBY³⁸ has shown that it must be considered as the breathing mode of the T₈O₁₂ subunit and can therefore be assigned to the D_{4R} breathing mode of zeolite A. According to Table 10, the 288- and 271-cm⁻¹ fundamentals are predominantly characterized by T-O(2) and T-O(3) stretching coordinates. They can therefore be assigned to breathing modes of the sodalite cage of zeolite A. T-O(1) and T-O(2) stretching motions form the 214-cm⁻¹ fundamental, which is an open part of the eight-membered ring of the α -cage of zeolite A and can therefore be assigned to the pore-opening vibration.

Acknowledgment. This work is financed by the Schweizerischer Nationalfonds zur Förderung der wissenschaftlichen Forschung (project NF 20-28528.90) and by the Schweizerisches Bundesamt für Energiewirtschaft (project BEW-EPA 217.307).

Appendix

A_{1g}

$$\mathcal{F}_{1,1} = f_R$$

$$\mathcal{F}_{2,2} = f_r + f_{rr} + 2f'_{rr}$$

$$\mathcal{F}_{3,3} = (f_{\alpha} + 2f_{\alpha\alpha}) + (f_{\beta} + 2f_{\beta\beta}) - 2(2f_{\alpha\beta} + f'_{\alpha\beta}) + 2f_{\Phi} + 4(f_{\alpha\Phi} - 2f_{\beta\Phi})$$

$$\mathcal{F}_{1,2} = \sqrt{3}f_{Rr}$$

$$\mathcal{F}_{1,3} = -\sqrt{3}(f_{R\alpha} - f_{R\beta})$$

$$\mathcal{F}_{2,3} = -(f_{r\alpha} + 2f'_{r\alpha}) + (2f_{r\beta} + f'_{r\beta}) - 2f_{r\Phi}$$

A_{2g}

$$\mathcal{F}_{4,4} = f_r$$

E_g

$$\mathcal{F}_{5,5} = f_r + f_{rr} - f'_{rr} \quad \mathcal{F}_{5,6} = f_{r\alpha} - f'_{r\alpha} \quad \mathcal{F}_{6,7} = -f_{\alpha\beta} + f'_{\alpha\beta}$$

$$\mathcal{F}_{6,6} = f_{\alpha} - f_{\alpha\alpha} \quad \mathcal{F}_{5,7} = -f_{r\beta} + f'_{r\beta} \quad \mathcal{F}_{6,8} = \sqrt{2}f_{\alpha\Phi}$$

$$\mathcal{F}_{7,7} = f_{\beta} - f_{\beta\beta} \quad \mathcal{F}_{5,8} = \sqrt{2}f_{r\Phi} \quad \mathcal{F}_{7,8} = -\sqrt{2}f_{\beta\Phi}$$

$$\mathcal{F}_{8,8} = f_{\Phi}$$

T_{1g}

$$\mathcal{F}_{9,9} = f_r - f_{rr} - f'_{rr} \quad \mathcal{F}_{9,10} = f_{r\alpha} - f'_{r\alpha}$$

$$\mathcal{F}_{10,10} = f_{\alpha} - f_{\alpha\alpha} \quad \mathcal{F}_{9,11} = f_{r\beta} - f'_{r\beta}$$

$$\mathcal{F}_{11,11} = f_{\beta} - f_{\beta\beta} \quad \mathcal{F}_{10,11} = f_{\alpha\beta} - f'_{\alpha\beta}$$

T_{2g}

$$\mathcal{F}_{12,12} = f_R$$

$$\mathcal{F}_{13,13} = f_r + f_{rr} + k^2f_{\Phi} - 2\sqrt{2}kf_{r\Phi}$$

$$\mathcal{F}_{14,14} = f_r - f_{rr} + f'_{rr} + \frac{k^2}{50}f_{\Phi}$$

$$\mathcal{F}_{15,15} = \frac{3}{2}(f_{\alpha} - f_{\alpha\alpha})$$

$$\mathcal{F}_{16,16} = \frac{1}{2}(f_{\alpha} + f_{\alpha\alpha}) + f_{\beta} - 2f_{\alpha\beta} + \frac{1}{18}f_{\Phi}$$

$$\mathcal{F}_{17,17} = (f_{\alpha} + f_{\alpha\alpha}) + (f_{\beta} + f_{\beta\beta}) - 2(f_{\alpha\beta} + f'_{\alpha\beta}) + \frac{16}{9}f_{\Phi} - \frac{16}{3}f_{\beta\Phi}$$

$$\mathcal{F}_{12,13} = f_{Rr}$$

$$\mathcal{F}_{12,14} = \sqrt{2}f_{Rr}$$

$$\mathcal{F}_{12,15} = 0$$

$$\mathcal{F}_{12,16} = -(f_{R\alpha} - f_{R\beta})$$

$$\mathcal{F}_{12,17} = -\sqrt{2}(f_{R\alpha} - f_{R\beta})$$

$$\mathcal{F}_{13,14} = \sqrt{2}f'_{rr} + \frac{\sqrt{2}k^2}{10}f_{\Phi} - \frac{k}{3}f_{r\Phi}$$

$$\mathcal{F}_{13,15} = (f_{r\alpha} - f'_{r\alpha}) - \sqrt{2}kf_{\alpha\Phi}$$

$$\mathcal{F}_{13,16} = -(f'_{r\alpha} - f'_{r\beta}) + \frac{\sqrt{2}k}{6}f_{\Phi} - \frac{1}{3}f_{r\Phi}$$

$$\mathcal{F}_{13,17} = -\sqrt{2}(f'_{r\alpha} - f_{r\beta}) + \frac{4k}{3}f_{\Phi} - \frac{4\sqrt{2}}{3}f_{r\Phi} - 2kf_{\beta\Phi}$$

$$\mathcal{F}_{14,15} = -\frac{1}{\sqrt{2}}(f_{r\alpha} - f'_{r\alpha}) - \frac{k}{3}f_{\alpha\Phi}$$

$$\mathcal{F}_{14,16} = -\frac{1}{\sqrt{2}}(f_{r\alpha} + f'_{r\alpha}) + \sqrt{2}f_{r\beta} + \frac{k}{30}f_{\Phi}$$

$$\mathcal{F}_{14,17} = -(f_{r\alpha} + f'_{r\alpha}) + (f_{r\beta} + f'_{r\beta}) + \frac{2\sqrt{2}k}{15}f_{\Phi} - \frac{\sqrt{2}k}{5}f_{\beta\Phi}$$

$$\mathcal{F}_{15,16} = \frac{1}{2}(f_{\alpha} - f_{\alpha\alpha}) - (f_{\alpha\beta} - f'_{\alpha\beta}) - \frac{1}{3}f_{\alpha\Phi}$$

$$\mathcal{F}_{15,17} = \sqrt{2}\left\{\frac{1}{2}(f_{\alpha} - f_{\alpha\alpha}) + \frac{1}{2}(f_{\alpha\beta} - f'_{\alpha\beta}) - \frac{4}{3}f_{\alpha\Phi}\right\}$$

$$\mathcal{F}_{16,17} = \sqrt{2}\left\{\frac{1}{2}(f_{\alpha} + f_{\alpha\alpha}) + f_{\beta\beta} - \frac{1}{2}(3f_{\alpha\beta} + f'_{\alpha\beta}) + \frac{2}{9}f_{\Phi} - \frac{1}{3}f_{\beta\Phi}\right\}$$

A_{2u}

$$\mathcal{F}_{18,18} = f_R$$

$$\mathcal{F}_{19,19} = f_r - f_{rr} + 2f'_{rr}$$

$$\mathcal{F}_{20,20} = (f_{\alpha} + 2f_{\alpha\alpha}) + (f_{\beta} + 2f_{\beta\beta}) - 2(2f_{\alpha\beta} + f'_{\alpha\beta})$$

$$\mathcal{F}_{18,19} = \sqrt{3}f_{Rr}$$

$$\mathcal{F}_{18,20} = -\sqrt{3}(f_{R\alpha} - f_{R\beta})$$

$$\mathcal{F}_{19,20} = -(f_{r\alpha} + 2f'_{r\alpha}) + (2f_{r\beta} + f'_{r\beta})$$

E_u

$$\mathcal{F}_{21,21} = f_r - f_{rr} - f'_{rr} \quad \mathcal{F}_{21,22} = f_{r\alpha} - f'_{r\alpha}$$

$$\mathcal{F}_{22,22} = f_{\alpha} - f_{\alpha\alpha} \quad \mathcal{F}_{21,23} = -f_{r\beta} + f'_{r\beta}$$

$$\mathcal{F}_{23,23} = f_{\beta} - f_{\beta\beta} \quad \mathcal{F}_{22,23} = -f_{\alpha\beta} + f'_{\alpha\beta}$$

T_{1u}

$$\mathcal{F}_{24,24} = f_R$$

$$\mathcal{F}_{25,25} = f_r + f_{rr} + f'_{rr} + \frac{k^2}{4}f_{\Phi} - \sqrt{2}kf_{r\Phi}$$

$$\mathcal{F}_{26,26} = f_r - f_{rr} + \frac{k^2}{50}f_{\Phi}$$

$$\mathcal{F}_{27,27} = \frac{3}{2}(f_{\alpha} - f_{\alpha\alpha})$$

$$\mathcal{F}_{28,28} = (f_{\alpha} + f_{\alpha\alpha}) + (f_{\beta} + f_{\beta\beta}) - 2(f_{\alpha\beta} + f'_{\alpha\beta}) + \frac{25}{18}f_{\Phi} + \frac{10}{3}(f_{\alpha\Phi} - f_{\beta\Phi})$$

$$\mathcal{F}_{29,29} = \frac{1}{2}(f_{\alpha} + f_{\alpha\alpha}) + f_{\beta} - 2f_{\alpha\beta} + \frac{25}{36}f_{\Phi} + \frac{5}{3}(f_{\alpha\Phi} - 2f_{\beta\Phi})$$

$$\mathcal{F}_{24,25} = \sqrt{2}f_{Rr}$$

$$\mathcal{F}_{24,26} = f_{Rr}$$

$$\mathcal{F}_{24,27} = 0$$

$$\mathcal{F}_{24,28} = -\sqrt{2}(f_{R\alpha} - f_{R\beta})$$

$$\mathcal{F}_{24,29} = -(f_{R\alpha} - f_{R\beta})$$

$$\mathcal{F}_{25,26} = \sqrt{2}f'_{rr} + \frac{\sqrt{2}k^2}{20}f_{\Phi} - \frac{k}{3}f_{r\Phi}$$

$$\mathcal{F}_{25,27} = -\frac{1}{\sqrt{2}}(f_{r\alpha} - f'_{r\alpha}) + \frac{k}{2}f_{\alpha\Phi}$$

$$\mathcal{F}_{25,28} = -(f_{r\alpha} + f'_{r\alpha}) + (f_{r\beta} + f'_{r\beta}) + \frac{5\sqrt{2}k}{12}f_{\Phi} - \frac{5}{3}f_{r\Phi} + \frac{\sqrt{2}k}{2}(f_{\alpha\Phi} - f_{\beta\Phi})$$

$$\mathcal{F}_{25,29} = -\frac{1}{\sqrt{2}}(f_{r\alpha} + f'_{r\alpha}) + \sqrt{2}f_{r\beta} + \frac{5k}{12}f_{\Phi} - \frac{5\sqrt{2}}{6}f_{r\Phi} + \frac{k}{2}(f_{\alpha\Phi} - 2f_{\beta\Phi})$$

$$\mathcal{F}_{26,27} = (f_{r\alpha} - f'_{r\alpha}) + \frac{\sqrt{2}k}{10}f_{\alpha\Phi}$$

$$\mathcal{F}_{26,28} = -\sqrt{2}(f'_{r\alpha} - f_{r\beta}) + \frac{k}{6}f_{\Phi} + \frac{k}{5}(f_{\alpha\Phi} - f_{\beta\Phi})$$

$$\mathcal{F}_{26,29} = -(f'_{r\alpha} - f'_{r\beta}) + \frac{\sqrt{2}k}{12}f_{\Phi} + \frac{\sqrt{2}k}{10}(f_{\alpha\Phi} - 2f_{\beta\Phi})$$

$$\mathcal{F}_{27,28} = \sqrt{2}\left\{\frac{1}{2}(f_{\alpha} - f_{\alpha\alpha}) + \frac{1}{2}(f_{\alpha\beta} - f'_{\alpha\beta}) + \frac{5}{6}f_{\alpha\Phi}\right\}$$

$$\mathcal{F}_{27,29} = \frac{1}{2}(f_{\alpha} - f_{\alpha\alpha}) - (f_{\alpha\beta} - f'_{\alpha\beta}) + \frac{5}{6}f_{\alpha\Phi}$$

$$\mathcal{F}_{28,29} = \sqrt{2}\left\{\frac{1}{2}(f_{\alpha} + f_{\alpha\alpha}) + f_{\beta\beta} - \frac{1}{2}(3f_{\alpha\beta} + f'_{\alpha\beta}) + \frac{25}{36}f_{\Phi} + \frac{5}{6}(2f_{\alpha\Phi} - 3f_{\beta\Phi})\right\}$$

T_{2u}

$$\mathcal{F}_{30,30} = f_r + f_{rr} - f'_{rr} \quad \mathcal{F}_{30,31} = f_{r\alpha} - f'_{r\alpha} \quad \mathcal{F}_{31,32} = f_{\alpha\beta} - f'_{\alpha\beta}$$

$$\mathcal{F}_{31,31} = f_{\alpha} - f_{\alpha\alpha} \quad \mathcal{F}_{30,32} = f_{r\beta} - f'_{r\beta} \quad \mathcal{F}_{31,33} = \sqrt{2}f_{\alpha\Phi}$$

$$\mathcal{F}_{32,32} = f_{\beta} - f_{\beta\beta} \quad \mathcal{F}_{30,33} = \sqrt{2}f_{r\Phi} \quad \mathcal{F}_{32,33} = \sqrt{2}f_{\beta\Phi}$$

$$\mathcal{F}_{33,33} = f_{\Phi}$$

References and Notes

- (1) Meier, W. M.; Olson, D. H. *Atlas of Zeolite Structure Types*; Butterworth: Stoneham, MA, 1988.
- (2) Breck, D. W. *Zeolite Molecular Sieves*; John Wiley & Sons, Inc.: New York, 1974.
- (3) Larsson, K. *Ark. Kemi* **1960**, *16*, 215.
- (4) Auf der Heyde, T. P. E.; Bürgy, H.-B.; Bürgy, H.; Törnroos, K. W. *Chimia* **1991**, *45*, 38.
- (5) Calzaferri, G.; Hoffmann, R. *J. Chem. Soc. Dalton Trans.* **1991**, 917.
- (6) Bornhauser, P.; Calzaferri, G. *Spectrochim. Acta* **1990**, *46A*, 1045.
- (7) Bärtsch, M.; Bornhauser, P.; Bürgy, H.; Calzaferri, G. *Spectrochim. Acta* **1991**, *47A*, 1627.
- (8) Bärtsch, M.; Bornhauser, P.; Calzaferri, G. *SPIE* **1992**, *1575*, 588.
- (9) Blackwell, C. S. *J. Phys. Chem.* **1979**, *83*, 3251, 3257.
- (10) de Man, A. J. M.; van Santen, R. A. *Zeolites* **1992**, *12*, 269.
- (11) Flanigen, E. M.; Khatami, H.; Szymanski, H. A. *Adv. Chem. Ser.* **1971**, *101*, 201.
- (12) Angell, C. L. *J. Phys. Chem.* **1973**, *77*, 222.
- (13) No, K. T.; Bae, D. H.; Jhon, M. S. *J. Phys. Chem.* **1986**, *90*, 1772.
- (14) Agaskar, P. A. *Inorg. Chem.* **1991**, *30*, 2707.
- (15) Bürgy, H.; Calzaferri, G. *Helv. Chim. Acta* **1990**, *73*, 698.
- (16) Blatter, F.; Schumacher, E. *J. Chem. Educ.* **1990**, *67*, 519.
- (17) Yang, B.; Morris, M. D.; Owen, H. *Appl. Spectrosc.* **1991**, *45*, 1533.
- (18) Schoen, C. L.; Sharma, S. K.; Helsley, C. E.; Owen, H. *Appl. Spectrosc.* **1993**, *47*, 305.
- (19) Wilson, E. B., Jr. *J. Chem. Phys.* **1939**, *7*, 1047; **1941**, *9*, 76.
- (20) McIntosh, D. F.; Peterson, M. R. *General Vibrational Analysis System*; QCPE Program No. QCMP067, 1988.
- (21) Gribov, L. A.; Orville-Thomas, W. J. *Theory and Methods of Calculation of Molecular Spectra*; John Wiley & Sons, Ltd.: New York, 1988.
- (22) Bornhauser, P. Ph.D. Thesis, Universität Bern, 1992.
- (23) Bürgy, H. Ph.D. Thesis, Universität Bern, 1991.
- (24) Teller, E. quoted by Angus, W. R.; et al. *J. Chem. Soc.* **1936**, 971.
- (25) Redlich, O. *Z. physikal. Chem. (B)* **1935**, *28*, 371.
- (26) Gussoni, M.; Zerbi, G. *J. Mol. Spectrosc.* **1968**, *26*, 485.
- (27) Wilson, E. B., Jr.; Decius, J. C.; Cross, P. C. *Molecular Vibrations*; McGraw-Hill Book Co.: New York, 1955.
- (28) Colthup, N. B.; Daly, L. H.; Wiberley, S. E. *Introduction to Infrared and Raman Spectroscopy*, 3rd ed.; Academic Press, Inc.: London, 1990.
- (29) Bellamy, L. J. *The Infra-red Spectra of Complex Molecules*, 3rd ed.; Chapman and Hall Ltd.: London, 1975.
- (30) Kriegsmann, H. Z. *Elektrochem. Ber. Bunsenges. physikal. Chem.* **1961**, *65*, 336, 342.
- (31) Arnett, R. L.; Crawford, B. L., Jr. *J. Chem. Phys.* **1950**, *18*, 118.
- (32) Morino, Y.; Kuchitsu, K. *J. Chem. Phys.* **1952**, *20*, 1809.
- (33) Bürgi, H.-B.; Bürgy, H.; Calzaferri, G.; Törnroos, K. W. *Inorg. Chem.* **1993**, *32*, 4914.
- (34) Calzaferri, G.; Imhof, R.; Törnroos, K. W. *J. Chem. Soc. Dalton Trans.* **1993**, 3741.
- (35) Smith, A. L. *Spectrochim. Acta* **1960**, *16*, 87.
- (36) Smith, A. L. *Spectrochim. Acta* **1963**, *19*, 849.
- (37) McIntosh, D. F.; Michaelian, K. H. *Can. J. Spectrosc.* **1979**, *24*, 1, 35, 65.
- (38) Höweler, U. *MOBY*, Molecular Modelling on the PC, Version 1.6F; Springer Verlag: Berlin, 1993.
- (39) Lazarev, A. N. *Vibrational Spectra and Structure of Silicates*; Consultants Bureau: New York, 1972.
- (40) Delfosse, J. M. *Nature* **1936**, *137*, 868.
- (41) Sverdlov, L. M.; Kovner, M. A.; Krainov, E. P. *Vibrational Spectra of Polyatomic Molecules*; John Wiley & Sons, Ltd.: Chichester, 1974.
- (42) Freeman, D. E.; Kent Wilson, M. Z. *Phys. Chem.* **1962**, *35*, 335.
- (43) Pluth, J. J.; Smith, J. V. *J. Am. Chem. Soc.* **1980**, *102*, 4704.
- (44) Beer, R.; Binder, F.; Calzaferri, G. *J. Photochem. Photobiol. A: Chem.* **1992**, *69*, 67.
- (45) Baumann, J.; Beer, R.; Calzaferri, G.; Waldeck, B. *J. Phys. Chem.* **1989**, *93*, 2292.
- (46) Boulet, H.; Brémard, C.; Le Maire, M. *J. Raman Spectrosc.* **1992**, *23*, 421.
- (47) Dutta, P. K.; Twu, J. *J. Phys. Chem.* **1991**, *95*, 2498.
- (48) Dutta, P. K.; del Barco, B. *J. Phys. Chem.* **1985**, *89*, 1861.
- (49) Geidel, E.; Böhlig, H.; Birner, P. *Z. Phys. Chem.* **1991**, *171*, 121.
- (50) The files for on-line inspection of the fundamentals of all molecules and fragments discussed in this article are available from the authors on request.
- (51) Dutta, P. K.; del Barco, B. *J. Phys. Chem.* **1988**, *92*, 354.
- (52) Beagley, B.; Titiloye, J. O. *Struct. Chem.* **1992**, *3*, 429.
- (53) Etchepare, J.; Merian, M.; Smetankine, L. *J. Chem. Phys.* **1974**, *60*, 1873.
- (54) de Kanter, J. J. P. M.; Maxwell, I. E.; Trotter, P. J. *J. Chem. Soc., Chem. Commun.* **1972**, 733.
- (55) Hess, A. C.; McMillan, P. F.; O'Keeffe, M. *J. Phys. Chem.* **1988**, *92*, 1785.
- (56) Raselli, A.-R. Ph.D. Thesis, Universität Bern, 1991.